Transcriptional memory of dFOXO activation in youth curtails later-life mortality through chromatin remodelling and Xbp1

Authors

Guillermo Martínez Corrales[1†], Mengjia Li[1†], Tatiana Svermova[1], Alex Goncalves[1], Diana Voicu[1], Adam J. Dobson[2], Tony D. Southall[3], Nazif Alic[1*].

[1]Institute of Healthy Ageing and the Research Department of Genetics, Evolution, and Environment, University College London, London WC1E 6BT, UK

[2]School of Molecular Biosciences, College of Medical, Veterinary and Life Sciences, University of Glasgow, Glasgow G12 8QQ, UK

[3]Department of Life Sciences, Imperial College London, London SW7 2AZ, UK

[†]These authors contributed equally

*Corresponding author: n.alic@ucl.ac.uk

Keywords: Transcriptional memory, dFOXO, physiological programming, ageing, *Drosophila*, chromatin remodelling, gene regulation, Xbp1, metabolism.

Abstract

A transient, homeostatic transcriptional response can result in transcriptional memory, programming subsequent transcriptional outputs. Transcriptional memory has great but unappreciated potential to alter animal ageing as animals encounter a multitude of diverse stimuli throughout their lifespan. Here we show that activating an evolutionarily conserved, longevity-promoting transcription factor, dFOXO, solely in early adulthood of female fruit flies is sufficient to improve their subsequent health and survival in mid- and late life. This youth-restricted dFOXO activation causes persistent changes to chromatin landscape in the fat body and requires chromatin remodellers such as the SWI/SNF and ISWI complexes to program health and longevity. Chromatin remodelling is accompanied by a long-lasting transcriptional programme that is distinct from that observed during acute dFOXO activation and includes induction of *Xbp1*. We show that this later-life induction of *Xbp1* is sufficient to curtail later-life mortality. Our study demonstrates that transcriptional memory can profoundly alter how animals age.

Introduction

Transcription is the first and key step in gene expression, the process linking a genotype to a phenotype. Orchestrated by transcription factors (TFs)[1], transcriptional programmes allow an animal to develop as well as to respond to its environment as an adult[2,3]. Indeed, transcriptional control has been studied within two such paradigms[4]: the programmatic paradigm of development and differentiation whereby permanent changes in gene expression determine cellular fates; and the homeostatic paradigm where cells maintain function by transiently reshaping gene expression. Similarly, TFs can be seen as either determining cell identity or allowing environmental responsiveness. However, these two paradigms cannot account for certain phenomena, such as transcriptional memory, where a homeostatic, transient transcriptional event produces a lasting, developmental-like impact on subsequent gene expression[5,6]. The mechanisms underpinning such transcriptional memory have attracted attention and are being intensely examined in cell systems, e.g. the response to galactose in the budding yeast[7] and the interferon response in mammalian cells in culture[6,8]. However, a broader understanding of the occurrence of transcriptional memory, its mechanisms and relevance for adult animal physiology is lacking.

Ageing is an intrinsic process that occurs in most animals[9] and results in increased disease susceptibility and reduced likelihood of survival with time[10,11]. In humans, old-age health is shaped by numerous environmental variables throughout our life course[12], and similar observations have been made in animal models[13-18]. However, the mechanisms underlying these long-term effects remain unclear. The involvement of transcriptional memory in this context has not been tested. Long-term effects of transcriptional memory have the potential to be especially important in ageing as animals encounter a variety of stimuli throughout their lifespan.

Forkhead Box O (FOXO) TFs maintain metabolic homeostasis in response to nutritional cues[3]. They are inhibited by the insulin/IGF signalling pathway and their activation promotes longevity in yeast, worms, flies, and likely humans[3,19-21]. In flies, this activity is tissue-specific, with adult-onset over-expression of *dfoxo* in fruit fly fat body (equivalent to mammalian liver and adipose tissue) and midgut (hereafter the gut, equivalent to the mammalian small intestine) promoting longevity; it is also sexually dimorphic extending female lifespan robustly, without a substantial effect on male longevity[22,23]. This fly model provides a highly tractable system with which to study transcriptional memory in the context of animal ageing, as it allows tissue-specific *dfoxo* induction to be switched on and off. Using this system, we set out to study transcriptional memory in the context of longevity in *Drosophila* females.

Results

dfoxo induction solely in early adulthood extends lifespan

We wanted to activate dFOXO in young adults and examine the effects of this activation in later life. *Drosophila* females are youthful in the first three weeks of adulthood; they are reproductively active, maintain essentially normal physiological function and are unlikely to die. Middle-aged flies, 20 to 60 days old in our healthy outbred background, lay substantially fewer eggs[24], experience functional impairments, e.g. loss of neuromuscular performance[25], but not high mortality. Older flies display substantial pathology, e.g. of the gut[26], and high mortality[27].

We transiently overexpressed *dfoxo* in the fat body and gut of adult females from day 2 to 23 of adulthood (hereafter referred to as *dfoxo*-switch, Fig. 1a) employing an inducible driver, *S106*[28] and feeding the inducer, RU^{486}. This driver did not show any substantial induction in the absence of RU^{486} (“leakiness”, as reported with other

GeneSwitch drivers[29-31]) and has been thoroughly characterised by us (Extended data Fig. 1a-c) and others[28,32]. Western blotting confirmed that dFOXO was increased in both organs during the induction with levels returning to normal within a week on food without RU[486] (Fig. 1b, c, Extended data Fig. 1d; levels in gut/fat body as expected for this driver, Extended data Fig. 1a). Interestingly, even though dFOXO levels did not persist, induction of *dfoxo* in young adults consistently extended subsequent lifespan, in line with previous reports (Fig. 1d, ref.[16,28]). The effect was not observed in *S106* or *UAS-dfoxo*-alone controls, indicating that it is not an RU[486]-feeding artefact (Extended data Fig. 2a and b). We observed the expected sexual dimorphism, with *dfoxo*-switch not extending male lifespan (Extended data Fig. 2c and d). Furthermore, *dfoxo* induction in the gut alone was insufficient for longevity (Extended data Fig. 2e), indicating that the fat body plays an essential role.

Can this long-term memory be established by any pro-longevity TF? Anterior open (Aop) is a transcriptional repressor whose chronic activation extends female lifespan from the same tissues as dFOXO's[32,33]. However, transiently inducing the activated form of *aop* (*aop*^{ACT}) in young adult females did not extend their subsequent lifespan (Extended data Fig. 2f), indicating that the ability to trigger a persistent effect is not a general characteristic of pro-longevity TFs.

Induction of *dfoxo* in the gut and fat body was previously shown to delay the age-related decline in neuromuscular performance[34], as measured by the fly's climbing ability (negative geotaxis assay)[35]. Similarly to its effects on survival, *dfoxo*-switch was sufficient to delay the age-related decline in climbing ability (detected as significant age-by-*dfoxo*-switch interaction, Extended data Fig. 2g). Combining data from three independent replicates allowed us to confirm that this beneficial effect persisted after

day 23, when *dfoxo* is already switched off (Fig. 1e, Supplementary Data 1). Hence, early-adulthood induction of *dfoxo* improves subsequent health.

Finally, to explicitly determine how long the effect of *dfoxo*-switch persists, we combined demographic data from four independent experiments, recording 985 fly deaths, in a mixed effects Cox Proportional Hazards (CPH) model. By estimating the Hazard Ratios (HR), we found that transient *dfoxo* induction in young adults significantly reduced the fly's risk of death in all subsequent periods by almost 50%. (Fig. 1f, Extended data Fig. 2h, Supplementary Data 1). Hence, our data show that induction of *dfoxo* in young adults generates a beneficial memory effect that persists in old age, influencing mortality half a lifetime later.

Benefits of *dfoxo*-switch require chromatin remodellers

Chromatin alterations are the prime candidate mechanisms for this lasting effect of *dfoxo*-switch as they can be triggered by TFs, persist over time, and are implicated in transcriptional memory[36,37]. To assess *in vivo* chromatin architecture, we employed the Assay for Transposase-Accessible Chromatin combined with next generation sequencing (ATAC-Seq) on dissected fat bodies and guts of *dfoxo*-switched females a week after *foxo* induction had ceased. As controls, we used their uninduced sisters, housed in parallel. We observed 3447 ATAC-Seq peaks in the fat body and 2906 in the gut samples (Supplementary Data 2). Their chromosomal distribution, sizes, and transcriptional start site (TSS) distance are shown in Extended data Fig. 3a-c. Dimensionality reduction, using t-distributed stochastic neighbour embedding (t-SNE), easily distinguished *dfoxo*-switched flies from controls based on the intensity of the ATAC-Seq peaks from the fat body but not from the gut samples (Fig. 2a). Indeed, DESeq2 analysis identified 81 regions that were differentially accessible to the

transposase in the fat body after *dfoxo*-switch but none in the gut at 10% false discovery rate (FDR) (Supplementary Data 2; examples of genomic regions with different characteristics and confirmed by qPCR are shown in Extended data Fig. 3d and e). 37% of these 81 peaks were 1kb from TSS and 72% were more accessible after *dfoxo*-switch, indicating opening of chromatin at promoter-proximal regions. Hence, dFOXO imprints persistent changes on chromatin landscape specifically in the adult fly fat body.

Interestingly, we found that 4 out of 81 genomic regions where chromatin accessibility was altered by *dfoxo*-switch overlapped regions that were previously characterised as bound by dFOXO in the fat body/gut using Chromatin Immunoprecipitation (ChIP) (Fig. 2b, ref.[32]). This relatively small overlap was statistically significant and prompted us to examine if dFOXO induction in early adulthood was sensitive to the levels of endogenous dFOXO. We found that *dfoxo*-switch performed in flies lacking endogenous *dfoxo* could extend their subsequent lifespan (Fig. 2c), indicating that dFOXO is unlikely to programme longevity by facilitating its own, subsequent access to chromatin.

To further characterise the genomic sites associated with these 81 regions of *dfoxo*-switch-responsive chromatin, we examined the 5176 ChIP datasets publicly available in ChIP-Atlas[38]. Focusing on histone modifications classified as either marking active or repressive chromatin (or “other”, Supplementary Data 2), we found that active marks tended to be enriched within our differentially accessible ATAC peak regions (Fig. 2d). Such active histone marks are often associated with a number of ATP-dependent chromatin remodellers that have vital and flexible roles in modulating chromatin structure, including formation of transcriptional memory in yeast and mediating the longevity effects of TF such as DAF-16, the worm FOXO[36,39,40].

We tested the involvement of proteins that are constituents of 10 of the 11 *Drosophila* ATP-dependent chromatin remodelling complexes (noted in Fig. 2e) in the physiological memory established by dFOXO, using validated RNAi constructs. We observed two different types of behaviour (Fig. 2e; all lifespans are presented in Extended data Fig. 4, data and analyses in Supplementary Data 2 and 3). Downregulation of *tip-60, Mi-2 and domino* during the first three weeks of adult life significantly increased subsequent mortality (after 23 days). Hence, the chromatin landscape set up in early adulthood by their chromatin remodelling and histone acetylation activity[41] can impact fly physiology at older ages. However, the detrimental effects of *tip60* and *domino* could be countered by co-expression of *dfoxo*, suggesting that dFOXO can extend lifespan independently from *tip60* and *domino* levels with the caveat that *tip60* and *domino* knockdowns may have been incomplete even though ubiquitous, constitutive expression of these RNAi constructs with the *daughterlessGal4* driver resulted in 100% pre-adult lethality, in concordance with previously published work[42]. The detrimental effect of *mi-2* was not fully counteracted by *dfoxo*, indicating it may be involved in its long-term effects.

On the other hand, RNAi against *moira, osa,* and *iswi* induced solely in young adults did not influence their subsequent lifespan while it did block the beneficial effects of *dfoxo*, demonstrating that they are required to form the physiological memory of dFOXO. Indeed, inducing either *mor* or *iswi* RNAi was sufficient to block the beneficial effects of *dfoxo*-switch on age-related decline in neuromuscular performance, whereas each RNAi alone did not reduce climbing performance (Extended data Fig. 5, Supplementary Data 2).

Additionally, we tested the involvement of *etl1* and *nejire* (*nej*), as they also have ATP-dependent chromatin remodelling functions[43] and *nej* (p300/CBP) interacts with

FOXO in different contexts[44,45]. We found that both silencing *etl1* and *nej* was able to block dFOXO's ability to programme lifespan, similarly to *mor, osa and iswi.* Note that RNAis against *mCherry*, *luciferase* and driver alone controls did not extend lifespan when induced on their own and did not block the lifespan extension produced by *dfoxo*-switch. Moreover, reducing the expression of *HP1*, a protein involved in transcriptional regulation and heterochromatin formation[46], did not have a significant effect on lifespan on its own, and did not alter the lifespan effect of *dfoxo*-switch.

Altogether, we identified specific members of chromatin remodelling complexes, namely moira, osa and iswi, as required for dFOXO to cause its beneficial, long-term effect on longevity and healthspan. These data reinforce the results of our ATAC-Seq analysis and indicate that transient activation of *dfoxo* in young adult females generates persistent changes in chromatin landscape that foster improved health and survival in mid- and late life.

A transcriptional programme is triggered by *dfoxo*-switch

The changes in chromatin landscape observed after *dfoxo*-switch are likely to underpin a long-term transcriptional programme. To investigate this, we profiled the transcriptomes of isolated fat bodies and guts from *dfoxo*-switched females a week after *dfoxo* induction had ceased, using their uninduced sisters as controls. Genes that were detected as responding to RU^{486} in driver-alone females (two in the fat body and 10 in the gut, Supplementary Data 4) were removed to avoid artifacts of RU^{486} feeding. 461 genes were differentially expressed after *dfoxo*-switch in the fat body (10% FDR, Fig. 3a and b, Supplementary Data 4), and only 87 in the gut. We confirmed by qPCR the expected fat body induction for three genes tested (*HDAC6*, *Pfk* and *Pepck1*; Extended data Fig. 6a). Interestingly, at least some of the transcriptional changes

204 could still be detected in whole flies at week 7 of adulthood (Extended data Fig. 6b),
205 indicating a long-lasting effect.

206 We assessed if the gene expression programme imposed after *dfoxo*-switch
207 (after *dfoxo* induction has ceased) is related to transcriptional changes observed
208 during acute *dfoxo* induction. We performed a meta-analysis of two published
209 transcriptomic studies[32,33], each performed in the same genetic background and with
210 the same experimental approaches and conditions as ours, to define a list of genes
211 differentially expressed during acute *dfoxo* induction in the adult fat body/gut (hereafter
212 referred to as *dfoxo*-acute) and compared it to our *dfoxo*-switch gene list. In the fat
213 body, only 10 genes were differentially expressed during both acute *dfoxo* induction
214 and a week after *dfoxo*-switch (Fig. 3b, Extended data Fig. 6c and d, Supplementary
215 Data 4). For these, the expression changes tended to be in the opposite direction
216 between acute *dfoxo* induction and *dfoxo*-switch (Extended data Fig. 6e). We
217 confirmed by qPCR that the levels of several transcripts differentially expressed after
218 *dfoxo*-switch were not responsive to acute *dfoxo* induction (Extended data Fig. 6f).
219 Overall, the persistent changes triggered by *dfoxo-switch* in the fat body did not appear
220 to be carried over from acute *dfoxo* induction in this organ. On the other hand, we
221 observed a significant overlap between acute and persistent transcriptional changes
222 in the gut (30 genes, Fig. 3b, Extended data Fig. 6c, d), indicating some, albeit limited
223 continuation of the acute transcriptional programme in this organ.

224 Interestingly, 98% of differentially expressed genes in the fat body were
225 upregulated (Fig. 3a). This is consistent with the detected increase in chromatin
226 accessibility in this organ, and the involvement of chromatin remodelling complexes
227 linked to transcriptional activation[47]. To further elucidate the links between differentially
228 open chromatin regions and differentially regulated genes, we used Binding and

Expression Target Analysis (BETA[48]) to integrate the two datasets (ATAC-Seq and RNA-Seq) and infer genes whose expression changed as the result of alterations in chromatin accessibility. We found that differentially accessible chromatin regions significantly explained upregulation of transcript levels (Extended data Fig. 6g) and identified 190 chromatin region-gene pairs, including 159 genes for which expression changes can be explained by altered chromatin accessibility in neighbouring genomic regions in the fat body; the majority of the genes were upregulated after the switch (Fig. 3c).

Our transcriptomic data are in line with the ATAC-Seq findings, both demonstrating that the effects of *dfoxo*-switch are different between the gut and the fat body. Indeed, transient induction of dFOXO can set up a distinct transcriptional programme in the fat body, likely mediated by changes to chromatin landscape in that organ, while it only leaves a small, residual of the original programme in the gut. For this reason, we focused our further investigation on the fat body.

***dfoxo*-switch flies exhibit a distinct metabolic profile**

To explore the physiological consequences of the long-term transcriptional programme in the fat body, we conducted Gene Ontology (GO) enrichment analysis on the entire set of genes differentially expressed in this organ after *dfoxo*-switch. We observed a strong overrepresentation of genes involved in metabolic pathways, particularly those of glucose metabolism (Fig. 4a, Extended data Fig. 7a). The overrepresented GO terms observed in the *dfoxo*-switch were different to those in *dfoxo*-acute (Extended data Fig. 7 and ref.[32,33]). As metabolic dysregulation is a consequence of ageing[10] and as TFs and chromatin structure play important roles in metabolic homeostasis[37], we interrogated the metabolic profiles of *dfoxo*-switch flies,

using liquid chromatography–mass spectrometry (LC/MS) analysis on whole-fly extracts. We detected 96 putative metabolites with levels significantly affected by *dfoxo*-switch, nine of which were identified using internal standards (Fig. 4b, Supplementary Data 5). Several could be mapped to the metabolic pathways that were transcriptionally regulated by *dfoxo*-switch in the fat body (Fig. 4c). We observed a significant increase of pyruvate and decrease of glycerol-3-phosphate in our *dfoxo*-switch flies compared to the controls, showing a concordance between transcriptional and metabolite changes in glucose metabolism, indicating that many of the metabolic changes, e.g. those in glucose metabolism, are likely occurring in the fat body. However, metabolic alterations in other tissues may also have been detected in our metabolomics analysis as it was performed on whole flies: e.g. the observed, high increase in acetylcholine may be coming from the brain.

This metabolic reprogramming mediated by *dfoxo*-switch may underly the long-term effects on longevity. Indeed, reduced expression of carbohydrate metabolism enzymes is a cause of ageing in *Drosophila* males and the over-expression of the genes encoding these enzymes can extend male lifespan[49]. We tested if transcriptionally upregulating the enzymes catalysing the committed and rate-limiting step in glycolysis, *Phosphofructokinase* (*Pfk)*, or gluconeogenesis, *Phosphoenolpyruvate carboxykinase 1* (*Pepck1*), is enough to affect female longevity. Both genes were found to be upregulated in the fat body after *dfoxo*-switch, but not during acute *dfoxo* induction (Extended data Fig. 6a and f, Supplementary Data 4). To mimic the effects of *dfoxo*-switch, we induced their expression from day 23 of adulthood (reverse-switch). Both this late-onset and chronic overexpression of *Pfk* or *Pepck1* produced either a modest or no effect on lifespan (Fig. 4d, e). Hence, our data are consistent with induction of *dfoxo* in young adults reprogramming metabolism in

278 later life. However, this may not be sufficient to explain fully the lifespan extension
279 observed.

280 **Induction of Xbp1 accounts for longevity after *dfoxo*-switch**

281 We sought to further understand the nature of the transcriptional programme
282 triggered by dFOXO activation in youth. 17 TFs were differentially expressed in the fat
283 body after *dfoxo*-switch. To examine if any one of them may drive transcriptional
284 changes after the switch, we sought DNA sequence motifs over-represented in the
285 promoters of all the genes differentially expressed in the fat body after *dfoxo*-switch
286 (Supplementary Data 6). The top three enriched motifs contained the ACGT sequence
287 (Fig. 5a), the core sequence bound by the human XBP1. Interestingly, our
288 transcriptomic data indicated that the fly *Xbp1* was upregulated after *dfoxo*-switch,
289 highlighting a dFOXO–Xbp1 relay as a potentially important component of the lifespan
290 programming by *dfoxo*-switch.

291 Xbp1 is an evolutionarily conserved TF that acts in one of the three branches of
292 the unfolded protein response[50]. Xbp1 activity is regulated post-transcriptionally
293 through unconventional splicing of its mRNA[51]. The transmembrane protein encoded
294 by *Inositol-requiring enzyme 1* (*Ire1* in *Drosophila*) catalyses the unconventional
295 splicing of the *Xbp1* mRNA in response to cues, e.g., accumulation of unfolded
296 proteins in the endoplasmatic reticulum (ER) or metabolic dysregulation. The spliced
297 *Xbp1* mRNA encodes a highly active TF that induces the expression of a plethora of
298 genes to alleviate proteostatic stress and regulate metabolism[51-56].

299 We further investigated the role of Xbp1 in the long-term benefits of *dfoxo-switch*.
300 Our RNA-Seq analysis couldn't distinguish between different *Xbp1* isoforms. Using
301 qPCR, we found that both the spliced and unspliced version of *Xbp1* mRNA (*Xbp1*^{S}

and *Xbp1*^{U} respectively) were indeed increased after *dfoxo*-switch in the fat body (Fig. 5b), indicating regulation of this TF at the level of transcription rather than splicing, which still results in increased levels of *Xbp1*^{S} mRNA. Consistent with activation of Xbp1 after the switch, we found a significant overlap in the genes whose expression depends on *Xbp1* in fly larvae[57] and those installed by *dfoxo*-switch in adult fat body (Fig. 5c). We could identify at least three genes, *hsc70-4*, *kay* and *eip75b*, for which the ectopic induction of *Xbp1*^{S} mimicked the effect of *dfoxo-switch* on their expression (Extended data Fig.8a and b). To check for physiological relevance of *Xbp1*^{S} upregulation, we examined the tolerance of our *dfoxo*-switched flies to orally administered tunicamycin, which induces proteostatic stress by inhibiting glycosylation of proteins in the ER[58]. We found a small but significant increase in tunicamycin resistance after *dfoxo*-switch [shown as reduced risk of death (HR) in Fig. 5d; survival in Extended data Fig. 8c and d, see Supplementary Data 6], consistent with activation of Xbp1, whereas we found no difference in starvation resistance (Extended data Fig. 8e and f) indicating a specific increase in proteostatic stress tolerance.

How does dFOXO regulate *Xbp1* expression? *Xbp1* was not upregulated during acute dFOXO induction, dFOXO binding has not been documented near the *Xbp1* locus in the fat body and we did not see significant changes in chromatin accessibility at this locus following *dfoxo-switch* (ref.[32,33], Extended data Fig. 6f, Extended data Fig. 3e), making it overall unlikely that *Xbp1* is a direct transcriptional target of dFOXO. Rather, *Xbp1* appears indirectly induced by *dfoxo*-switch. To test weather this indirect induction requires the same chromatin remodellers that are required for the longevity effect of the *dfoxo-switch*, we knocked down *mor* or *iswi* during the switch: this prevented the upregulation of *Xbp1* (Fig. 5e). Similarly, tunicamycin tolerance after *dfoxo*-switch was dependent on *mor* and *iswi*: knockdown of either during *dfoxo*

induction in the first three weeks of adulthood blocked any beneficial effect of *dfoxo*-switch on tunicamycin tolerance in week 4 (Figure 5d; note mor^{RNAi} alone reduced tunicamycin tolerance, Extended data Fig. 8g-j). Hence, like longevity, *Xbp1* induction and the resulting proteostatic-stress tolerance after *dfoxo-switch* are also dependent on chromatin remodellers. This prompted us to directly query the role of *Xbp1* in longevity.

Xbp1 has been intensely studied in the context of proteostatic stress and has been linked to metabolism and animal longevity more recently[59-61]. Therefore, we tested whether the fly orthologue also promotes longevity when expressed in a time-restricted manner by inducing either the full, splicable *Xbp1* mRNA ($Xbp1^{RA}$) or specifically the spliced $Xbp1^{S}$ [57]. To mimic the effects of *dfoxo*-switch, we induced expression only from day 23 of adulthood (reverse-switch). Both this late-onset and chronic overexpression of $Xbp1^{RA}$ or $Xbp1^{S}$ were sufficient to extend lifespan, recapitulating the longevity of *dfoxo*-switched flies (Fig. 5f and g). Hence, our data are consistent with induction of *dfoxo* in young adults resulting in increased, later expression of *Xbp1*, which improves survival of these flies in mid- and late life.

dfoxo-switch may counteract transcriptional ageing

Chromatin disorganisation and gene expression dysregulation occur during ageing in multiple species[62]. We were interested to see if *dfoxo*-switch-responsive transcripts show age-related deregulation. To define the ageing fat body transcriptome, we analysed transcriptomic changes occurring in female fat bodies from day 10 to day 50 using published data[63]. Interestingly, we found that the genes differentially expressed after *dfoxo*-switch were significantly enriched for those affected by ageing ($p=8.9x10^{-12}$, *one-sided hypergeometric test*). For most, the

direction of change induced by ageing is counteracted by *dfoxo*-switch (Fig. 6a). The transcriptional dysregulation that occurs with age is correlated to the transcriptional profile ensuing from *Xbp1* loss-of-function (Fig. 6b), indicating a decline in the expression of Xbp1-target genes with age that is remedied by *Xbp1* induction after *dfoxo-switch*.

As similar age-related changes can occur in different species[64,65], we identified mouse orthologues of the genes differentially expressed in the fat body after the *dfoxo*-switch. We examined if this set of genes is enriched for genes susceptible to age-related dysregulation, based on a recently published mouse ageing transcriptome study[65] and focusing on the organs equivalent to the fly fat body: mouse liver and adipose tissue. The expression of these orthologues was more likely to be susceptible to ageing generally (Fig. 6c), albeit without a predictable directionality (Extended data Fig. 9). Hence, the genes whose expression maintains a memory of past *dfoxo* induction tend to be dysregulated with age. In the fly fat body, the long-term programme initiated by dFOXO appears to counteract age-related dysregulation.

Discussion

We employed a tissue-specific, inducible system of *in vivo dfoxo* induction in the fruit fly to show that dFOXO activation in youth can trigger transcriptional memory to curtail later life mortality. FOXO TFs are at crossroads of multiple pathways signalling changes in external environment and the internal milieu[21]. Hence, alteration in FOXO activity may underly the risks and benefits of early life experiences, such as nutrition or exercise, that are increasingly documented to programme health and survival later in life[5,11,16,17,66]. Understanding the mechanisms and relevance of transcriptional

programming to animal physiology will have a profound impact on strategies ensuring human health throughout the life course.

Our study highlights the importance of chromatin architecture set in youth for later ageing. Firstly, we demonstrated that specific chromatin remodellers, those linked to histone acetylation (*mi2, dom* and *tip60*), are crucial in early adulthood to determine subsequent longevity in a wild-type female. Indeed, histone modifications, including histone acetylation, are recognised as important regulators of animal longevity[41,67-71]. Our findings support and add to this as we found that even a short-time downregulation of these proteins in early life can dramatically curtail lifespan, regardless of their levels later in life. Secondly, we identified specific chromatin remodelling complexes required by dFOXO to extend lifespan, indicating that the activity of e.g. SWI/SNF and ISWI in youth promotes later longevity.

FOXOs are canonically considered as homeostatic TFs, allowing transient responses to a changing environment. The SWI/SNF complex is known to be essential for the worm FOXO orthologue, DAF-16, to extend lifespan[40] and for transcriptional memory of galactose exposure in yeast[7]. However, the link between the roles of SWI/SNF in transcriptional memory and lifespan had not been made. There is increasing evidence that FOXO TFs make long-lasting alterations to chromatin landscape, both via direct recruitment of chromatin organisers and indirect changes in their expression[16,72-74]. Our study indicates that these combined features of FOXOs, homeostatic responsiveness and the ability to organise chromatin, result in their ability to orchestrate transcriptional memory with long-term consequences for animal physiology. This aspect of FOXO function is likely to be relevant to mammals.

FOXO TFs are well known regulators of glucose metabolism and metabolic gene expression[75]. We did not find that manipulating the expression of carbohydrate

metabolic enzymes could recapitulate the effects of dFOXO. Rather, our study implicates a dFOXO-to-Xbp1 transcriptional relay as an important component of longevity programming by dFOXO activation in youth: Xbp1 acts after *dfoxo* induction has ceased to curtail later-life mortality, most likely by counteracting the age-related loss of proteostasis, as documented in other contexts[59,60]. *Xbp1* transcriptional induction appears to be an indirect consequence of prior dFOXO activation in the fat body, likely as a secondary effect of primary transcriptional or metabolic changes. Interestingly, complex links between XBP1, metabolism, proteostasis and ageing are still emerging[76-79]. Particularly, new roles of Xbp1 in lipid metabolism have been reported in *Drosophila*. Zhao and colleagues demonstrated that the Ire1/Xbp1 axis mobilises lipids in response to chronic starvation, and this effect is dependent on dFOXO inactivation[76]. It will be interesting to understand in more detail how Xbp1 activation is impacted by dFOXO activity, chromatin structure and transcriptional and metabolic reprogramming.

Age-related changes in chromatin organisation are a key hallmark of ageing[10]. They are pervasive across species, cell types and timescales and are accompanied by transcriptional dysregulation[37]. While this dysfunction in epigenetic and transcriptional control of gene expression has often been speculated as causal in ageing, direct evidence has only recently started emerging[71,80]. Our work adds to this body of evidence that preserving or restoring a youthful epigenetic and transcriptional programme by a relatively short intervention promotes health and longevity, highlighting that such resetting can occur even before the visible onset of ageing.

Methods

Fly husbandry

The Dahomey wild-type stock was obtained in 1970 in what is today Benin and has been maintained in large population cages on a 12L:12D cycle at 25°C. The white Dahomey (*wDah*) and vermillion Dahomey (*vDah*) stocks were derived by incorporation of the w^{1118} or v^{1} mutation, respectively, into the Dahomey background by extensive backcrossing. *wDah* population used is *Wolbachia*-free and females from this background were used in all crosses to generate experimental flies. Mutants and transgenes were backcrossed into *wDah* (or *vDah* for BDSC TRiP lines) population for at least six generations, except for *etl1, mi2, tip60, dom, nej and HP1* RNAi lines, UAS-*Pepck1*, *UAS-Xbp1*^{RA} and UAS-X*bp1*^{S}. Stock maintaince and experimental conditions: 25°C, a 12h:12h light/dark cycle, constant 60% humidity and standard sugar/yeast/agar (SYA) medium unless otherwise stated[81]. The chromatin complexes chosen for the epistasis experiments shown in Fig. 2 were selected under the FlyBase category *Chromatin Remodelling Complexes (ATP-dependent)*, curated by FlyBase curators[82]. All fly stocks are listed in Supplementary Data 7.

Lifespan assays

Lifespan assays were performed as described in ref.[83]. In brief, crosses were set up in cages containing grape juice agar and live yeast, flies were allowed to mate and then embryos were collected for < 22-hr, washed in PBS and seeded into bottles at ~20 µl per bottle to achieve standard density[81,84]. Females, allowed to mate for 48h, were used in experiments, unless otherwise noted. Flies were subsequently lightly anaesthetized with CO_2 and split into 15 per vial. Experimental vials contained either

food with RU (RU+) at 200μM RU[486] (Sigma, #M8046) or control food (RU-, containing the equivalent volume of EtOH vehicle). Vials were kept in DrosoFlippers (drosoflipper.com) and flies were transferred to fresh food three times a week, when deaths/censors were recorded. For the switch group, RU+ food was supplied from day 2 to day 23 and the flies were switched to control food for the rest of the experiment. The reverse switch group were supplied with RU+ food from day 23. Data were collected using Excel. Details of statistical analyses and number of flies per condition (n) are provided in figure legends or Supplementary Data. Log-rank tests of survivorship and Cox proportional hazards (CPH) analysis to obtain Hazard Rations (HR) were performed using R (R Core Team). Experimental trial was used as a random effect when required. GraphPad Prism 6 (GraphPad, La Jolla, CA) was used for graphic representation of survival curves. Lifespan data are provided in Supplementary Data 1, 2, 3, 5 and 6.

Negative geotaxis (climbing) assays

Climbing assays were performed as described previously[85]. In brief, at indicated times flies were transferred to empty vials placed in DrosoFlippers to allow climbing of 2 vial heights. The same cohort was continuously assayed. After acclimatising for 30 min, flies were gently tipped to the bottom of the vial and video recorded for 20 s. Video stills from the same time point (15 s; when young wild-type flies nearly reach maximum height) were analysed in Fiji[86] and fly coordinates exported to R (R Core Team). If the height could not be determined, the fly was not used in the analysis. Top and bottom 5% of data per condition/timepoint were excluded to protect from outliers. Data were analysed with a mixed effects LM (using flipper as random effect) and the two-sided

F-test p values obtained with the anova() function in R were reported. Climbing data are provided in Supplementary Data 1 and 2.

Tunicamycin and starvation stress assays

Tunicamycin (2 mg l^{-1} in DMSO, Cell Signaling) was added to sugar and agar food. In control treatments, equivalent volumes of the vehicle alone were added. For starvation assays, flies were placed in vials containing 1% agarose only. In both tunicamycin and starvation assays, 30 day-old, *dfoxo*-switch or control flies (1 week after recovery) were used. The vials were check for dead flies once or twice a day until no living flies remained. All statistical analyses were performed in R (R Core Team). Survival data are provided in Supplementary Data 6.

Cloning and generation of UAS-pepck1 fly line

Pepck1 coding sequence (CDS) was PCR amplified from *wDah* cDNA to include CACC preceding the ATG, was transferred to pENTR™/D-TOPO® vector using the pENTR™ /D-TOPO® Cloning Kit and transformed into NEB® Stabl Competent *E. coli* (c30401). The correct clone was confirmed by DNA sequencing at Source Biosciences. Gateway LR reactions were conducted between the *pENTR-pepck* entry clone and *pGW.AttB* destination vector and transformed into library efficiency competent cells (Invitrogen #C404003). The *UAS-pepck* construct was confirmed by restriction enzyme digestion and sequencing. The construct were injected into embryos and integrated through the phiC31 integrase-mediated transgenesis[87] at the Department of Genetics Fly Facility (University of Cambridge) (https://www.flyfacility.gen.cam.ac.uk/Services/Microinjectionservice). *phiC31* expressing stock *nos-int; attP2* (Stock 13-18) was provided by the Cambridge fly facility.

Immunostaining

Fat bodies and guts were dissected from 1 week-old *S106>nL8-GFP* females kept for 5 days on RU+ or RU- food in ice-cold PBS and fixed with 4% paraformaldehyde for 20 min at room temperature. Tissues were washed 3 times in PBS + 0.1% Triton and blocked with 5% Bovine Serum Albumin for 2h. Incubations with the primary antibody (anti-GFP, 1:1000, 488 conjugate, Invitrogen) were performed overnight at 4°C. After mounting in Vectashield (Vector Laboratories), the samples were imaged using a Zeiss LSM AxioObserver confocal microscope (Zeiss, Oberkochen, Germany) and processed with Zeiss ZEN software and Adobe Illustrator. Details about the antibodies used in this study are provided in the Supplementary Data 7.

Western blotting

Midguts and fat bodies (associated with the abdominal cuticle) were dissected, transferred to 12.5% trichloroacetic acid, homogenized with glass beads (#G8772) and spun for 15 min at 14,000 rpm at 4°C. Pellets were washed twice with 1M Tris and the resulting pellet was resuspended in 50µl of LDS sample buffer (50% LDS sample buffer, 100 mM DTT, in nuclease-free water). Protein samples were then separated in 8% Poly-Acrylamide gels (Acrylamide/Bis-Acrylamide solution, Sigma A7168) following manufacturer's instructions, and transferred to a nitrocellulose membrane. Membranes were blocked, incubated at 4°C overnight with primary antibodies (anti-dFOXO 1:5000, anti-Actin 1:1000) in 5% skimmed milk (Millipore #70166), washed and probed with secondary antibodies (1:10000) for 2h at room temperature. Details about the antibodies used in this study are provided in the Supplementary Data 7. Anti-

dFOXO and anti-Actin were applied sequentially to the same membrane. Densitometric analysis of blot images was carried out using Fiji software[86].

RNA-Sequencing

Midguts and fat bodies (associated with the abdominal cuticle) were dissected in ice-cold PBS. Dissected tissues were placed directly into ice-cold Trizol (ThermoFisher Scientific #15596026). Five experimental replicates were obtained per condition, each containing twelve fat bodies or guts. RNA was extracted by Trizol-chloroform extraction, quantified on a NanoDrop 2000c spectrophotometer, and integrity was assessed on an Agilent Bioanalyzer. Poly(A) RNA was pulled down using NextFlex Poly(A) beads (PerkinElmer NOVA-512981). RNA fragments were given unique molecular identifiers and libraries were prepared for sequencing using NextFlex Rapid Directional qRNAseq v2 reagents, (barcode sets C and D, PerkinElmer NOVA-5130-14 and NOVA-5130-15) and 16 cycles of PCR. Individual and pooled library quality, size and molarity were assessed on an Agilent Bioanalyzer and quantified with a Qubit spectrophotometer. Libraries were pooled at equal molarity in NextFlex resuspension buffer. Due to poor RNA or library yield/quality, three samples were not sequenced. Sequencing was performed by the UCL Cancer Institute, using an Illumina NextSeq 500 instrument, with a single-end 75bp sequencing length.

ATAC-Sequencing

The ATAC-Seq protocol was adapted from ref.[88]. Fat bodies and guts were dissected as for RNA-Seq. Three experimental replicates were obtained per condition, each containing forty fat bodies or guts (approximately 50k nuclei were employed for each replicate). After dissection, midguts were placed in 1ml of HB buffer (15mM Tris-

HCl pH 7.4, 15mM NaCl, 1M KCl, 0.2mM EDTA pH 8, 0.2mM EGTA pH 7, with Roche complete mini protease inhibitor (#11836170001), in nuclease-free water). Mid guts were homogenised with a Dounce homogeniser on ice and filtered with a 20µm filter. Nuclei were spun at 3500g, 4°C for 5 min and washed with HB buffer twice. Then, nuclei were resuspended in 50µl of PBS. For the fat bodies, they were placed after dissection in 50µl of lysis buffer (10mM Tris-HCl ph 7.4, 10mM NaCl, 3mM gCl2, 0.1% IGEPAL CA-630). They were mixed by pipetting vigorously 10 times, and the supernatant was transferred to a new tube. Nuclei were spun at 3500g, 4°C for 5 min, and resuspended with lysis buffer. Then, nuclei were resuspended in 200µl of PBS. Nuclear DNA was tagmented by resuspending in Illumina buffer TD (from Illumina Nextera kit, kind gift from Richard Jenner and Maria Vila De Mucha, UCL Cancer Institute) with 1.6µg of Tn5 produced as described in ref.[89] to a total volume of 50µl. Reactions were incubated at 36°C for 30 minutes, pausing every 10 minutes for gentle manual agitation. DNA was eluted immediately using the Qiagen minelute PCR purification kit, and the whole eluate was amplified by PCR (10µl DNA eluate, 10µl H_2O, 2.5µl 25µM forward primer, 2.5µl 25 µM reverse primer (primer sequences are provided in Supplementary Data 7), 25 µl NEBNext Ultra II Q5 Master Mix (M0544). After an initial extension step (5 minutes at 72°C, 30 seconds at 98°C), tagmented DNA was amplified by 5 initial cycles of PCR (10s at 98°C, 30s at 63°C, 1min at 72°C). To determine the number of subsequent PCR cycles required to reach exponential phase per library, 5µl of the PCR reaction were amplified by qPCR (with 4.41µl nuclease-free H_2O, 0.25µl forward primer, 0.25µl reverse primer, 0.09µl 100x SYBR green, 5µl NEBNext Ultra II Q5 Master Mix; in a PCR program comprising 30s at 98°C followed by 20x cycles of 10 s at 98°C, 30 s at 63°C, 1 min at 72°C). Each initial PCR reaction was then cycled for the number of additional cycles required indicated by

qPCR. DNA was eluted and size-selected using AMPure XP beads, quantified on a Qubit spectrophotometer, and library size and integrity were checked on an Agilent Bioanalyser. Individual library molarity was calculated from the Bioanalyser size estimate and Qubit density measurement, and libraries were pooled at equal molarity in NextFlex resuspension buffer.

qPCR

RNA samples were converted to cDNAs using SuperScript II Reverse Transcriptase (ThermoFisher Scientific, #18064014) and Oligo-dT. qPCR was performed on an Applied Biosystems QuantStudio 6 Flex real-time PCR instrument with Fast SYBR Green PCR Master Mix (Applied Biosciences #4385612), with primers supplied by Thermo Fisher (all primer sequences used in this study are shown in Supplementary Data 7), relative to a standard curve comprising a pool of all samples and the instrument's standard PCR cycle. *Actin* was used for normalisation in expression analysis unless its quantity was suspected of changing with one of the experimental conditions, in which case *tubulin* or *eIF1A* were used instead. Mixed effects LM (dissection batch as random effect) was used in expression qPCR analysis, where each model was sequentially reduced removing all the insignificant terms and the two-sided *F-test* p values obtained with the anova() function reported.

ATAC-seq and RNA-seq data processing and analysis

The following workflow was applied for all the raw sequencing data [raw data have been deposited in Gene Expression Omnibus GEO (GSE183542)]. Read quality was assessed using FastQC. ATAC reads were trimmed using Trimmomatic version 0.33 to improve alignment rates. Both RNA-Seq and ATAC-Seq reads were aligned to the *Drosophila melanogaster* genome (r6.19) using HiSAT2, version 2.1.0. For RNA-

Seq, alignments were counted with featureCounts over exons per gene. Preliminary principal component analysis of *dfoxo*-switch RNA-seq showed that one midgut and one fat body of S106>*dfoxo* +RU^{486} sample, originating from the same flies, clustered away from all other samples, and were removed from subsequent analyses. One further *dfoxo*-switch gut sample had low gene counts assigned ($<10^6$) and was also removed. ATAC-Seq peaks were called with MACS2 version 2.1.2 for each tissue/treatment. The peaks were combined per tissue and per-peak counts for each sample were generated using featureCounts. Differential gene expression and differential ATAC signal intensities were assessed with DESeq2 and the ihw packages in R (R core team). The effect of RU^{486} feeding in the first three weeks followed by one week recovery was assessed in S106>*dfoxo* and S106 flies, separately. Gene Ontology (GO) term analysis was performed by topGO package in R[90], and KEGG pathway analysis was performed using DAVID[91]. The circos plot of peak distribution was generated by circlize in R[92]. The bar plots showing peaks distance related to TSS were generated by ChIPseeker in R[93]. Other plots were generated using ggplot2 in R. Data associated with ATAC-Seq and RNA-Seq analyses, including analyses results, are given in Supplementary Data 2 and 4.

BETA analysis

BETA analysis was carried out in BETA 1.0.7[48] with default parameters. To explore the potential chromatin region-gene interactions comprehensively, differentially open ATAC-Seq peaks with a p-value < 0.05 (244 peaks) were regarded as binding data input. Expression data input include the *dfoxo*-switch fat body RNA-seq gene list, FDR 10% as threshold was applied to specify differentially expressed

genes. The *Drosophila melanogaster* genome R6 (r6.19) was used for genome annotation.

RNA-seq and ChIP-seq analysis from public datasets

Biological information of the following RNA-seq datasets were obtained from GEO, and raw data (fastq files) were downloaded from Sequence Read Archive (SRA) employing SRA Toolkit (version 2.11). Datasets include *Drosophila* female fat body gene expression in different ages (GSE130158), gene expression of *Xbp1* mutant flies at larval stage 2 (GSE99676). Raw gene counts data from mouse gene expression datasets obtained from different ages and tissues were obtained from the Tabula Muris Senis project's website (https://twc-stanford.shinyapps.io/maca/). 5176 processed peak files of the Publicly available *Drosophila* ChIP-seq datasets following the uniform processing protocol were obtained from ChIP-Atlas[38]. The annotations of each peak file were also obtained from ChIP-Altas.

Changes in gene expression with age analysis

To assess transcriptomic impacts of age, gene expression was modelled as a function of age as a continuous covariate in a linear model, fitted by DESeq2. Daily gene expression change was calculated from a previously published *Drosophila* female fat body gene expression dataset[63], and mouse weekly gene expression change was calculated from the dataset from[65], where the DESeq2 linear model was fitted in every combination of sexes and tissues. Comparison of gene expression list from different studies was performed within their DESeq2 results. Hypergeometric tests were used to quantify overlap significance between differential expressed gene lists. Linear regressions of Log2 fold change were used to estimate gene expression correlation.

Comparisons to published ChIP datasets and acute dFOXO transcriptome meta-analysis

To compute overlap between *dfoxo*-switch ATAC-peaks and publicly available *Drosophila* ChIP peaks, permutation tests (n = 10000), which generated random peaks based on given length and numbers, were performed in regioneR package[94] and FDR10% was used as the threshold for further analyses. Meta-analysis of the induced *dfoxo* gene expression was conducted using the metafor package in R[95] where random effect model with maximum likelihood (ML) estimators was used.

Motif analysis

TF binding motifs enriched in differentialyl expressed *dfoxo*-switch gene list (FDR 10%) were calculated using the R package RcisTarget[96]. Motif-ranking dataset used the "dm6-5kb-upstream-full-tx-11species". Motif-annotation dataset used the motifAnnotations_dmel embedded in the package. Functions were run using default settings.

Metabolite extraction

Five 30-day-old female flies (whole) were collected per replicate for metabolite extraction. 7 technical replicates were used for the RU- condition and 8 for RU switch condition. They were briefly anesthetised in CO_2 and snap-frozen in liquid nitrogen prior to metabolite extraction. Frozen flies were suspended in 200µL of Chloroform/Methanol (analytical grade) /Water (1:3:1 ratio) at 4°C containing glass beads and were homogenized at 4°C. Samples were then centrifuged for 3 minutes at 13,000g at 4°C and 180µL of supernatant was subtracted and stored at -80°C for

further analysis by LC–MS. A pooled sample was generated by combining 20µl of each sample, to be used as a quality control sample in the LC–MS procedure.

LC/MS

LC/MS was performed by Glasgow Polyomics, as described before[97]. Hydrophilic interaction liquid chromatography (HILIC) used a Dionex UltiMate 3000 RSLC system (Thermo Fisher Scientific, Hemel Hempstead, UK) with a ZIC-pHILIC column (150 mm × 4.6 mm, 5 µm column, Merck Sequant) maintained at 30°C. A linear gradient (20 mM ammonium carbonate in water, A and acetonitrile, B) was used to elute the samples over 24 min at a flow rate of 0.3 ml/min as follows: min 0: 20% A, 80% B, min 15: 80% A, 20% B, min 15: 95% A, 5% B, min 17: 95% A, 5% B, min 17 20% A, 80% B, min 26 20% A, 80% B. Injection volume was 10µl. The samples were kept at 5°C before injection. For the MS analysis, a Thermo Orbitrap QExactive (Thermo Fisher Scientific) was operated in polarity switching mode. MS settings were: Resolution 70,000, AGC 1e6. m/z range 70–1050, Sheath gas 40, Auxiliary gas 5 Sweep gas 1, Probe temperature 150°C, Capillary temperature 320°C. For positive mode ionisation: source voltage +3.8 kV, S-Lens RF Level 30.00, SLens Voltage -25.00 (V), Skimmer Voltage -15.00 (V), Inject Flatapole Offset -8.00 (V), Bent Flatapole DC -6.00 (V). For negative mode ionisation: source voltage-3.8 kV.

Metabolomics data analysis

Raw data was uploaded by Glasgow Polyomics to PiMP (http://polyomics.mvls.gla.ac.uk). Peaks Data used for subsequent analysis was generated by PIMP. Metabolite identification was performed in MetaboAnalyst 5.0[98] using the following parameters: Missing value estimation by K-nearest neighbour, filtering by standard deviation, sample normalization by sum, data transformation by

log (generalized logarithm transformation or glog) and data scaling by autoscaling (mean-centered and divided by the standard deviation of each variable). Significant peaks were identified by t-test in MetaboAnalyst, and p-values were adjusted by Benjamini-Hochberg method (FDR) using R (R core team). Peaks with an FDR < 0.1 were assigned as significant. Peaks were assigned to their corresponding metabolites regarding their mass and retention time (RT). Metabolite annotation was assigned to putative metabolites to the signal based on matching their mass and RT with database or library entries. Metabolite identification was performed by direct comparison of the properties of an authentic standard ran in parallel. Metabolomics raw data, relevant metadata and protocols are available in the MetaboLights repository (ref.[99], study identifier MTBLS3251). Data and results tables from metabolomic analysis are given in Supplementary Data 5.

Statistics and reproducibility

No statistical method was used to predetermine sample size. Sample size selection was informed by and is consistent with those employed in previous research in the field[16,20,23,100]. The investigators were not blinded to allocation during experiments and outcome assessment as one or few researcher(s) tended to perform the entire experiment and blinding was not practical. Treatment group allocation of experimental conditions was randomised in such a way as to avoid any potential confounding effects. Few data were excluded: 1) due to technical failure 2) two RNA-Seq samples based on principal component analysis (detailed above), 3) trimming of 5% top/bottom for climbing data to avoid outlier impact (detailed above), 4) censors from lifespan experiments due to accidental killing or escape (numbers reported). Statistical tests for each experiment are mentioned in their corresponding figure captions with additional detail provided in Methods. Adjustments for multiple testing

were used for ‘omics data (RNA-Seq, ATAC-Seq, metabolomics) as reported. Normal distribution of residuals for LMs was confirmed by visual inspection; no formal testing of assumptions underlying the statistical tests was performed. All statistical analyses were performed in R or RStudio (R Core Team), versions 3.6.3 – 4.1.0 .

Data availability statement

Raw RNA-Seq and ATAC-Seq data are available from the Gene Expression Omnibus GEO (accession number GSE183542). Metabolomics data are available from the MetaboLights repository (study identifier MTBLS3251). All other data are available as Supplementary Data provided with the manuscript or can be made available by the corresponding author on reasonable request.

Publicly available data used in the study were:

1) *Drosophila* female fat body gene expression in different ages (GSE130158) and gene expression of *Xbp1* mutant flies at larval stage 2 (GSE99676) both obtained from https://www.ncbi.nlm.nih.gov/geo/
2) Raw gene counts data from mouse gene expression datasets obtained from different ages and tissues were obtained from the Tabula Muris Senis project’s website https://twc-stanford.shinyapps.io/maca/
3) 5176 processed peak files of the Publicly available *Drosophila* ChIP-seq datasets following the uniform processing protocolas well as the annotations of each peak file were obtained from https://chip-atlas.org/
4) Fly genome release and annotation were obtained from https://flybase.org/

Acknowledgements

We thank HD. Ryoo, L. Partridge and T. Niccoli for providing fly stocks; C. Regnault from Glasgow Polyomics for assistance with Metabolomics analysis; The University of Cambridge Department of Genetics Fly Facility for generating fly stocks; Y. Zhao for help with Tn5 synthesis; A. Vieira and J. Uriach for technical assistance; and the IHA members for support, comments, and discussion throughout this project. Fly stocks were obtained from the Bloomington Drosophila Stock Center. This work was supported by the Biotechnology and Biological Sciences Research Council [BB/R014507/1] grant to TDS and NA; and the Medical Research Council [MR/S033939/1] grant to AJD. The funders had no role in study design, data collection and analysis, decision to publish or preparation of the manuscript. NA dedicates this work to the memory of his mother, Ema Hodžić.

Author contributions

NA and TDS contributed to study and experimental design. GMC, ML, TS, AG, DV and AD performed experimental work, and GMC, ML, AD, DV and NA analysed the data. NA, GMC and MJ wrote the manuscript with inputs from AD and TDS.

Competing interests

The authors declare no competing interests

Figure captions

Fig. 1. Transient expression of *dfoxo* in early adulthood extends subsequent lifespan. **a** Experimental setup: 2-day-old *S106>dfoxo* females were placed on food containing RU^{486} to induce *dfoxo* expression until day 23 when they were placed back on food without RU^{486} (*dfoxo*-switch flies, red arrow). Their sisters were not fed RU^{486} at any time (grey arrow). **b** Western-blot quantifications of gut or fat body dFOXO during induction (day 7) and one week after (day 30). Boxplot – quantiles; whiskers – extremes; overlay – individual data points. $N = 4$ biologically independent samples; day 7: effect of RU^{486} $p = 0.035$, tissue $p = 0.0018$, RU^{486}-by-tissue interaction $p = 0.33$; day 30: RU^{486} $p = 0.169$, tissue $p = 0.048$, interaction $p = 0.13$; *linear model* (*LM*). **C** Representative western blots against dFOXO and Actin. * non-specific binding by dFOXO antibody in fat body samples. FB – fat body, G – gut. Same-day samples on the same membrane, sequentially probed with anti-dFOXO and anti-Actin. Image source data – Extended data Fig. 1d. **d** *dfoxo*-switch lifespan. Control $n = 139$ dead/3 censored flies, *dfoxo*-switch $n = 141$ dead/4 censored flies, $p = 2 \times 10^{-10}$, *log-rank test*. **e** Height climbed by *dfoxo*-switch compared to control females, from day 23, pooled from three independent trials. Individual trials – Extended data Fig. 2g. *N* – individual flies; boxplots – quantiles; whiskers – extremes; overlay – individual data points. Effect of *dfoxo*-switch $p = 0.5648$, age $p < 10^{-4}$, age-by-*dfoxo*-switch interaction $p = 0.0118$, *mixed-effects LM*. **f** Hazard ratios (HRs) – points, and 95% confidence intervals (CI) – whiskers, from a *mixed-effects Cox Proportional Hazards* (CPH) model on the combined events (985 dead, 9 censored) from four independent trials. Individual trials - Extended data Fig. 2h. HRs < 1 indicate switched flies exhibit lower risk of death compared to uninduced controls. Detailed statistical analyses for **b** and **f** are shown in Supplementary Data 1.

Fig. 2. *dfoxo*-switch induces persistent changes in chromatin structure and requires chromatin remodellers for longevity. a tSNE plots generated from the intensities of all detected ATAC peaks in *foxo*-switch and control fat bodies and guts, after variance stabilizing transformation (VST). **b** Venn diagram showing overlap between fat body ATAC peaks with significantly altered accessibility after dfoxo-switch (81 peaks) and previously described dFOXO-bound ChIP peaks (1361 peaks, p = 0.008, *one-sided permutation test*). **c** *Δdfoxo S106>dfoxo* switch lifespans. Control n = 139 dead/4 censored flies, *dfoxo*-switch n = 136 dead/9 censored flies, p = 1.95 x 10^{-19}, *log-rank test*. **d** Proportion of histone modification ChIP datasets deposited in ChIP-atlas, classified as underpinning gene activation, repression, or other, for the datasets where the ChIP peaks significantly overlap (10% FDR) our ATAC peaks that show differential accessibility caused by *dfoxo*-switch (right bar; 89 marking activation, 22 repression and 8 other) or those for which this overlap is not significant (left bar; 702 marking activation, 545 repression and 98 other), p = 5.893 x 10^{-6}, *Pearson's Chi−squared test*. See also Supplementary Data 2. **e** HRs – points, and 95% CIs – whiskers, indicate the relative risk of death in switched flies compared to their uninduced sisters after day 23 and were determined for *dfoxo*-switch when *dfoxo* is induced in the presence of RNAi constructs targeting the indicated genes (right) or the same RNAi constructs transiently expressed on their own (left). HRs < 1 indicate a lower risk of death compared to uninduced controls, HRs > 1, the opposite. P value for HRs being significantly different from 1, *CPH models*. Grey vertical area highlights the results for *mor*, *osa* and *iswi.* Individual lifespans and demographic details - Extended data Fig. 4 and Supplementary Data 3.

Fig. 3. A unique transcriptional programme is triggered in the fat body by *dfoxo*-switch a Volcano plots showing the effect of *dfoxo*-switch on transcripts in the fat body and the gut with differentially expressed genes (FDR 10%) shown in red. **b** Overlaps of differentially expressed genes between the effects of *dfoxo*-switch and acute *dfoxo* induction in the fat body and gut. Differential expression in *dfoxo*-acute set is based on a meta-analysis of two previously described datasets that profiled the transcriptome during dFOXO induction (essentially day 7). Overlap p-values from *one-sided hypergeometric test*. **c** Heatmaps of *dfoxo*-switch gene – *dfoxo*-switch peak pairs assigned with BETA. The left shows ATAC-seq and the right RNA-seq signal intensities (after VST and scaling to the control condition for each peak/gene). Each column is a biologically independent sample. Genes down-regulated in RNA-Seq are presented at the bottom.

Fig. 4. *dfoxo*-switch flies exhibit a distinct metabolic profile. a Top 5 GO terms and KEGG pathways for all the genes differentially expressed after *dfoxo*-switch in the fat body. See Supplementary Data 4. **b** Relative changes in metabolites comparing females after *dfoxo*-switch with their controls. Identified metabolites are labelled and marked in red. See Supplementary Data 5. **c** Metabolic map highlighting the enzymes with significant changes in mRNA levels after *dfoxo*-switch (red lines) and significantly altered, identified metabolites (grey and red dots). The pathways in which both differentially expressed genes and altered metabolites are involved are annotated. **d** *Pfk*-reverse switch lifespan. *S106>Pfk* females were fed food containing RU^{486} chronically or from day 23 (reverse switch). Control n = 127 dead/10 censored flies, *Pfk*-reverse switch n = 119 dead/3 censored flies, p = 0.03 vs control, *log-rank test*, *Pfk*-chronic n= 127 dead/10 censored flies p = 0.007 vs control, *log-rank test*. **e**

Pepck1-reverse switch lifespan. *S106>Pepck1* females were fed food containing RU^{486} chronically or from day 23 (reverse switch). Control n = 141 dead/5 censored flies, *Pepck1*-reverse switch n = 115 dead/5 censored flies, p = 0.97 vs control, *log-rank test*, *Pepck1*-chronic n= 91 dead/4 censored flies p = 0.46 vs control, *log-rank test*.

Fig. 5. Xbp1 activation accounts for longevity resulting from *dfoxo*-switch. a The three top-ranked motifs identified as enriched within the promoters of genes differentially expressed after *dfoxo*-switch in the fat body. Underlined - ACGT core sequence bound by Xbp1; NES – Normalised Enrichment Score. **b** qPCR quantifications of $Xbp1^{s}$ and $Xbp1^{u}$ transcripts in *dfoxo*-switched fat bodies at day 30. *N* – biologically independent samples; boxplots – quantiles; whiskers – extremes; overlay – individual data points. Effect of *dfoxo*-switch $p < 7\times10^{-4}$, effects of transcript or *dfoxo*-switch-by-transcript interaction p > 0.05, *mixed effects LM*. **c** Overlap of differentially expressed genes between *dfoxo*-switch in the fat body and *Xbp1* mutant larvae. Overlap p-value from *one-sided hypergeometric test*. **d** HRs - points, and 95% CI – whiskers, from *CHP models* showing the relative risk of death during tunicamycin feeding initiated after a week of recovery from *dfoxo*-switch or *dfoxo*-switch co-induced with RNAi against *mor* or *iswi*. HR < 1 indicates a lower risk of death compared to uninduced controls. P value from *CPH models*. See Extended data Fig. 7g-j. **e** qPCR quantifications of $Xbp1^{s}$ and $Xbp1^{u}$ in fat bodies a week after *dfoxo*-switch or *dfoxo*-switch performed together with induction of *mor* or *iswi RNAi*. *N* – biologically independent samples; boxplots – quantiles; whiskers – extremes; overlay – individual data points. Effect of *dfoxo*-switch p = 0.035, *dfoxo* + $iswi^{RNAi}$-switch p>0.05, *dfoxo* + mor^{RNAi}-switch $p < 4\times10^{-4}$; effects of transcript or switch-by-transcript interaction p >

844 0.05; *mixed effects LM*s. **f** Lifespans of *S106>Xbp1^{RA}* females fed food containing
845 RU^{486} chronically or from day 23 (reverse switch). Control n = 105 dead/1 censored
846 flies; *Xbp1^{RA}* -reverse switch n = 106 dead/1 censored flies p = 0.021 vs control, *log-*
847 *rank test; Xbp1^{RA}* -chronic n = 138 dead/2 censored flies p = 0.0265 vs control, *log-*
848 *rank test*. **g** *Lifespans of S106>Xbp1^{S}* females. Control n = 145 dead/3 censored flies;
849 *Xbp1^{S}* -reverse switch n = 143 dead/0 censored flies, p = 6.03 x 10^{-5} vs control, *log-*
850 *rank test*; *Xbp1^{S}* -chronic n = 154 dead/0 censored flies p = 0.0001 vs control, *log-rank*
851 *test*.

852

853 **Fig. 6. *dfoxo*-switch counteracts age-related transcriptional dysregulation. a**
854 Relationship between log_2Fold Change (FC) in gene expression caused by ageing and
855 *dfoxo*-switch in *Drosophila* fat body, for genes differentially regulated by both *dfoxo-*
856 switch and age. β = -8.23, p < 2.2 x10^{-16}, *LM*. **b** Relationship between FC in gene
857 expression caused by ageing and *xbp1* null mutant (*xbp1$^{-/-}$*), for genes differentially
858 regulated by both *xbp1$^{-/-}$* and age. β = -8.64, p = 0.00589, *LM*. Points – individual
859 genes; line – line of best fit, shaded – 95% CI for the line. **c** Overlaps of mouse
860 orthologues of genes differentially expressed after *dfoxo*-switch in flies and genes
861 differentially expressed with age in the mouse. Grey – mouse genes that show age-
862 related expression changes, red – mouse orthologues of fly genes that are
863 differentially expressed after *dfoxo*-swich in the fat body. P-values from *one-sided*
864 *hypergeometric tests*.

865

Extended Data Figure Captions

Extended Data Fig. 1 Experimental setup – expression.
a Expression pattern of *UAS-n8-GFP*, driven with the *S106* driver in 7 day-old female guts and fat bodies. All images were taken at exactly the same laser conditions under the confocal microscope, to allow the comparison of GFP levels between the two tissues. Scale bars are 50µm. **b** representative example of a *S106* > *n8-GFP* fat body, induced or not with RU486, under different imaging conditions to (a), allowing a better view of GFP induction in fat body cells. Scale bars are 50µm. **c** Quantification of *dfoxo* mRNA levels in *S106* alone and *S106 UAS-dfoxo* both uninduced. Boxplots – quantiles; whiskers – extremes; overlay – individual data points. N = 4, 3 (left to right), p = 1, *unpaired two-sided t-test.* **d** Uncropped images of the western-blot membranes shown in Fig.1c.

Extended Data Fig. 2 *dfoxo*-switch – additional lifespans, and climbing ability measurements.
a Driver-alone (*S106*) RU^{486}-switch control lifespan. Control n = 150 dead/1 censored fly, switch n = 148 dead/0 censored flies, p = 0.69, *log-rank test*. **b** UAS-*dfoxo* alone RU^{486}-switch control lifespan. Control n = 135 dead/2 censored flies, switch n = 136 dead/12 censored flies, p = 0.86, *log-rank test*. **c** Male driver-alone (*S106*) RU^{486}-switch control lifespan. Control n = 126 dead/12 censored flies, RU^{486}-switch n = 143 dead/6 censored flies, p = 0.49, *log-rank test.* **d** Male *dfoxo*-switch lifespan. Control n = 154 dead/6 censored flies, *dfoxo*-switch n = 142 dead/8 censored flies, p = 0.72, *log-rank test*. **e** *TiGS>dfoxo*-switch lifespan. Control n = 128 dead/3 censored flies, *dfoxo*-switch n = 141 dead/4 censored flies, p = 0.85, *log-rank test*. **f** *S106>aop^{Act}*-switch lifespan. Control n = 145 dead/7 censored flies, *aop^{Act}*-switch n = 147 dead/2 censored flies, p = 0.00274, *log-rank test*. **g** Experimental trials of the negative geotaxis assays of *dfoxo*-switch and control that were combined for the analysis presented in Fig. 1e. N = individual flies, boxplots – quantiles; whiskers – extremes; overlay – individual data points. Experiment 1: effect of *dfoxo*-switch p = 0.008, age $p < 10^{-4}$, age-by-*dfoxo*-switch interaction p = 0.0008, *mixed-effects LM*. Experiment 2: effect of *dfoxo*-switch p > 0.05, age $p < 10^{-4}$, age-by-*dfoxo*-switch interaction p = 0.033, *mixed-effects LM*. Experiment 3: effect of *dfoxo*-switch p > 0.05, age $p < 10^{-4}$, age-by-*dfoxo*-switch interaction p = 0.07, *mixed-effects LM*. **h** Experimental trials of *S106>dfoxo*-switch lifespans used for the analyses presented in Fig 1f. Experimental trial 1: control n = 61 dead/0 censored flies, *dfoxo*-switch n = 76 dead/0 censored flies, p = 0.009, *log-rank test*. Experimental trial 2: shown in Fig. 1d. Experimental trial 3: control n = 145 dead/1 censored fly, *dfoxo*-switch n = 145 dead/1 censored fly, $p = 1.72189 \times 10^{-5}$, *log-rank test*. Experimental trial 4: control n = 125 dead/0 censored flies, *dfoxo*-switch n = 145 dead/2 censored flies, $p = 6.05 \times 10^{-9}$, *log-rank test*.

Extended Data Fig. 3 ATAC-Seq – additional information.
a Schematic distribution of the ATAC peaks on the four main *Drosophila* chromosomes. Additional peaks were detected on contigs and are not shown. **b** Violin plots showing the size of all ATAC peaks detected in the gut and fat body, and in the significantly differentially accessible peaks in the fat body. **c** Distribution of the distance of ATAC peaks from a transcriptional start site (TSS). Proportion of peaks in each distance category are presented from 5' to 3' relative to the TSS. **d** ATAC-qPCR of the levels of sequences near the *MED1 locus* where an ATAC-Seq peak opened by *dfoxo*-

switch was detected, near *Prosap* where a peak unaltered by *dfoxo*-switch was detected, and *Sox21b* region which contained no peak in ATAC-Seq. Boxplots – quantiles; whiskers – extremes; overlay – individual data points. N = 3 biologically independent samples; effect of *dfoxo*-switch: *MED1* p=0.00024, *Prosap* p=0.59, *Sox21b* p=0.76, pairwise comparisons with *two-sided unpaired t-tests with pooled SD*. **e** ATAC-qPCR signal intensity for regions near the *Xbp1* locus within a peak detected by ATAC-Seq (3'end of the gene) or two regions within the promoter of *Xbp1*. The levels were normalized to *Prosap*. Boxplots – quantiles; whiskers – extremes; overlay – individual data points. N = 3 biologically independent samples, effect of region p = 0.0011, effect of *dfoxo*-switch p > 0.05, *mixed effects LM*.

Extended Data Fig. 4 *dfoxo*-switch dependence on chromatin remodelers – lifespan. Lifespan curves of the switch in *S106>dfoxo & RNAi* (**a**) or *S106>RNAi* (**b**) with indicated RNAi lines. These were used to generate the analysis shown in Fig. 2e. P values are obtained comparing control vs RU^{486}-switch conditions (after day 23, *log-rank test*). Detailed statistical analyses including number of flies per experiment are shown in Supplementary Data 2 and 3.

Extended Data Fig. 5 *dfoxo*-switch dependence on chromatin remodelers – climbing ability.
a Negative geotaxis assay of *dfoxo*-switch + *mor* RNAi at all ages, combining two independent trials. Effect of the switch p = 0.6, age $p < 10^{-4}$, age-by-switch interaction p = 0.36, *mixed-effects LM*. **b** Negative geotaxis assay of *dfoxo*-switch + *iswi* RNAi at all ages . Effect of the switch p = 0.12, age $p < 10^{-4}$, age-by-switch interaction p = 0.14, *mixed-effects LM*. **c** Negative geotaxis assay of *mor* RNAi switch at all ages. Effect of the switch p = 0.02, age $p < 10^{-4}$, age-by-switch interaction p = 0.006, *mixed-effects LM*. **d** Negative geotaxis assays of *iswi* RNAi switch at all ages. Effect of the switch p = 0.62, age $p < 10^{-4}$, age-by-switch interaction p = 0.49, *mixed-effects LM*. N - individual flies, boxplots – quantiles; whiskers – extremes; overlay – individual data points. The negative geotaxis assays of *dfoxo*-switch that were performed at the same time are shown in Extended Data Fig. 2g, experiments 2 and 3.

Extended Data Fig. 6 RNA-Seq – additional information.
a qPCR quantification of transcripts detected as differentially expressed in our RNA-Seq data (*HDAC6*, *Pfk*, *Pepck1*) in fat bodies after *dfoxo*-switch. Effect of *dfoxo* p = 0.0055, transcript p = 0.0386, and *dfoxo*-switch-by-transcript interactions p = 0.032, *mixed effects LM*. **b** qPCR quantifications of *dfoxo*-switch targets (*MED1*, *HDAC6*, $Xbp1^{s}$, *Pfrx)* at week 7 in *dfoxo*-switch females. Effect of *dfoxo*-switch p = 0.0133, effect of transcript or *dfoxo*-switch-by-transcript interaction p > 0.05, *mixed effects LM*. N – biologically independent samples; boxplots – quantiles; whiskers – extremes; overlay – individual data points. **c** and **d** Overlaps of sets of differentially expressed genes between *dfoxo*-switch (red circles) and *dfoxo*-acute (grey circles) in the fat body and gut employing previously published gene lists. Overlap p-values from *one-sided hypergeometric test*. **e** Bar plot comparing the $\log_2$ fold change of the transcripts in common between the sets of genes differentially regulated by *dfoxo*-acute (meta analysis) and by *dfoxo*-switch. **f** qPCR quantifications of transcripts during acute induction of *dfoxo* in the fat body. *HDAC6*, *Pfk*, $Xbp1^{s}$, $Xbp1^{u}$ were examined as they are all differentially expressed after *dfoxo*-switch in the fat body (RNA-Seq analysis and qPCR confirmation shown elsewhere). N – biologically independent samples; boxplots – quantiles; whiskers – extremes; overlay – individual data points. Effects of

RU^{486}, transcript or RU^{486}-by-transcript interaction $p > 0.05$, *mixed effects LM* . **g** Activating/Repressing Function prediction in BETA applying *one-tailed Kolmogorov-Smirnov* test. Differentially accessible ATAC peaks explained transcriptional activation ($p=2.97x10^{-46}$) and repression ($p=0.028$) after *dfoxo*-switch.

Extended Data Fig. 7 Additional GO terms enrichment analysis.
Top 5 GO terms and KEGG pathways for genes differentially expressed (DE) **a** exclusively after *dfoxo*-switch and **b** exclusively during *dfoxo*-acute induction in the fat body. Note that no significant GO enrichment was observed in the set of genes that are differentially expressed in both *dfoxo*-switch and *dfoxo*-acute.

Extended Data Fig. 8 Involvement of *Xbp1* in the effects of *dfoxo*-switch – additional information.
a qPCR quantification of transcripts whose levels are increased after *dfoxo*-switch in fat bodies (*Hsc70-4*, *Eip75b*, *kay*) in female *S106>Xbp1^{s}* fat bodies, with or without RU^{486} induction. Effect of RU^{486} $p = 0.0088$, effect of transcript or RU^{486}-by-transcript interaction $p > 0.05$, *mixed effects LM*. **b** qPCR quantifications of the same transcripts in fat bodies after *dfoxo*-switch. Effect of RU^{486} $p = 0.0001$, effect of transcript or RU^{486}-by-transcript interaction $p > 0.05$, *mixed effects LM*. N – biologically independent samples; boxplots – quantiles; whiskers – extremes; overlay – individual data points. **c** Survival of *dfoxo*-switch flies challenged with tunicamycin after 1 week of recovery (day 30; control n = 142 dead/0 censored, *dfoxo*-switch n = 129 dead/0 censored, p = 0.001, *log-rank* test). **d** Same for driver-alone (control n = 114 dead/0 censored, switch n = 131 dead/0 censored, p = 0.21, *log-rank* test). **e** Starvation assay of 30-day-old *dfoxo*-switch flies (control n = 142 dead/0 censored, *dfoxo*-switch n = 151 dead/0 censored, p = 0.67, *log-rank* test). **f** Same for driver-alone (control n = 149 dead/0 censored, switch n = 149 dead/0 censored, p = 0.07, *log-rank* test). **g-j**. Survival in the presence of tunicamycin a week after the switch in: *S106>mor^{RNAi}* (control n = 141 dead/1 censored, switch n = 154 dead/0 censored, $p < 6x10^{-7}$, *log-rank* test), *S106>iswi^{RNAi}* (control n = 146 dead/0 censored, switch n = 145 dead/0 censored, p = 0.60, *log-rank* test), *S106>dfoxo mor^{RNAi}* (control n = 140 dead/0 censored, switch n = 139 dead/0 censored, $p < 8x10^{-7}$, *log-rank* test), *S106>dfoxo iswi^{RNAi}* (control n = 153 dead/0 censored, switch n = 148 dead/0 censored, p = 0.079 *log-rank* test).

Extended Data Fig. 9 Age-related expression changes in the mouse – additional information.
Relationship between the expression changes triggered by *dfoxo*-switch in the fly fat body and the expression changes caused by ageing of their mouse orthologues (FDR 10%) in the functionally equivalent organs in the mouse. Points – genes; lines with shading – line of best fit and 95% CI; grey – those that are not significantly changed with age, red – those that are significantly changed with age. None of the organs show significant correlation between age-related change and d*foxo*-switch change ($p > 0.05$, *LM*).

References

1 Spitz, F. & Furlong, E. E. Transcription factors: from enhancer binding to developmental control. *Nature reviews genetics* **13**, 613-626 (2012).

2 Lasko, P. Patterning the Drosophila embryo: A paradigm for RNA-based developmental genetic regulation. *Wiley Interdisciplinary Reviews: RNA* **11**, e1610 (2020).

3 Webb, A. E. & Brunet, A. FOXO transcription factors: key regulators of cellular quality control. *Trends in biochemical sciences* **39**, 159-169 (2014).

4 Latchman, D. S. Transcription factors: an overview. *The international journal of biochemistry & cell biology* **29**, 1305-1312 (1997).

5 D'Urso, A. & Brickner, J. H. Epigenetic transcriptional memory. *Current genetics* **63**, 435-439 (2017).

6 Siwek, W., Tehrani, S. S., Mata, J. F. & Jansen, L. E. Activation of clustered IFNγ target genes drives cohesin-controlled transcriptional memory. *Molecular cell* **80**, 396-409. e396 (2020).

7 Bheda, P., Kirmizis, A. & Schneider, R. The past determines the future: sugar source history and transcriptional memory. *Curr Genet* **66**, 1029-1035, doi:10.1007/s00294-020-01094-8 (2020).

8 Kamada, R. *et al.* Interferon stimulation creates chromatin marks and establishes transcriptional memory. *Proceedings of the National Academy of Sciences* **115**, E9162-E9171 (2018).

9 Jones, O. R. *et al.* Diversity of ageing across the tree of life. *Nature* **505**, 169-173 (2014).

10 López-Otín, C., Blasco, M. A., Partridge, L., Serrano, M. & Kroemer, G. The hallmarks of aging. *Cell* **153**, 1194-1217 (2013).

11 Partridge, L., Deelen, J. & Slagboom, P. E. Facing up to the global challenges of ageing. *Nature* **561**, 45-56 (2018).

12 Kuh, D., Karunananthan, S., Bergman, H. & Cooper, R. A life-course approach to healthy ageing: maintaining physical capability. *Proceedings of the Nutrition Society* **73**, 237-248 (2014).

13 Dearden, L., Bouret, S. G. & Ozanne, S. E. Nutritional and developmental programming effects of insulin. *Journal of Neuroendocrinology* **33**, e12933 (2021).

14 Obata, F., Fons, C. O. & Gould, A. P. Early-life exposure to low-dose oxidants can increase longevity via microbiome remodelling in Drosophila. *Nature communications* **9**, 1-12 (2018).

15 Bitto, A. *et al.* Transient rapamycin treatment can increase lifespan and healthspan in middle-aged mice. *elife* **5**, e16351 (2016).

16 Dobson, A. J. *et al.* Nutritional programming of lifespan by FOXO inhibition on sugar-rich diets. *Cell reports* **18**, 299-306 (2017).

17 Catterson, J. H. *et al.* Short-term, intermittent fasting induces long-lasting gut health and TOR-independent lifespan extension. *Current Biology* **28**, 1714-1724. e1714 (2018).

18 Hahn, O. *et al.* A nutritional memory effect counteracts the benefits of dietary restriction in old mice. *Nature metabolism* **1**, 1059-1073 (2019).

19 Murphy, C. T. The search for DAF-16/FOXO transcriptional targets: approaches and discoveries. *Experimental gerontology* **41**, 910-921 (2006).

20 Corrales, G. M. & Alic, N. Evolutionary conservation of transcription factors affecting longevity. *Trends in Genetics* **36**, 373-382 (2020).
21 Martins, R., Lithgow, G. J. & Link, W. Long live FOXO: unraveling the role of FOXO proteins in aging and longevity. *Aging cell* **15**, 196-207 (2016).
22 Hwangbo, D. S., Gersham, B., Tu, M.-P., Palmer, M. & Tatar, M. Drosophila dFOXO controls lifespan and regulates insulin signalling in brain and fat body. *Nature* **429**, 562-566 (2004).
23 Giannakou, M. E. *et al.* Long-lived Drosophila with overexpressed dFOXO in adult fat body. *Science* **305**, 361-361 (2004).
24 Koch, R. E., Phillips, J. M., Camus, M. F. & Dowling, D. K. Maternal age effects on fecundity and offspring egg-to-adult viability are not affected by mitochondrial haplotype. *Ecology and evolution* **8**, 10722-10732 (2018).
25 Augustin, H. & Partridge, L. Invertebrate models of age-related muscle degeneration. *Biochimica et Biophysica Acta (BBA)-General Subjects* **1790**, 1084-1094 (2009).
26 Rera, M., Azizi, M. J. & Walker, D. W. Organ-specific mediation of lifespan extension: more than a gut feeling? *Ageing research reviews* **12**, 436-444 (2013).
27 Piper, M. D. & Partridge, L. Drosophila as a model for ageing. *Biochimica et Biophysica Acta (BBA)-Molecular Basis of Disease* **1864**, 2707-2717 (2018).
28 Giannakou, M. E. *et al.* Dynamics of the action of dFOXO on adult mortality in Drosophila. *Aging cell* **6**, 429-438 (2007).
29 Poirier, L., Shane, A., Zheng, J. & Seroude, L. Characterization of the Drosophila gene-switch system in aging studies: a cautionary tale. *Aging cell* **7**, 758-770 (2008).
30 Scialo, F., Sriram, A., Stefanatos, R. & Sanz, A. Practical recommendations for the use of the GeneSwitch Gal4 system to knock-down genes in Drosophila melanogaster. *Plos one* **11**, e0161817 (2016).
31 Parkhitko, A. A. *et al.* A genetic model of methionine restriction extends Drosophila health-and lifespan. *Proceedings of the National Academy of Sciences* **118** (2021).
32 Alic, N. *et al.* Interplay of dFOXO and two ETS-family transcription factors determines lifespan in Drosophila melanogaster. *PLoS Genet* **10**, e1004619 (2014).
33 Dobson, A. J. *et al.* Longevity is determined by ETS transcription factors in multiple tissues and diverse species. *PLoS genetics* **15**, e1008212 (2019).
34 Alic, N. *et al.* Cell-nonautonomous effects of dFOXO/DAF-16 in aging. *Cell reports* **6**, 608-616 (2014).
35 Gargano, J. W., Martin, I., Bhandari, P. & Grotewiel, M. S. Rapid iterative negative geotaxis (RING): a new method for assessing age-related locomotor decline in Drosophila. *Experimental gerontology* **40**, 386-395 (2005).
36 Kundu, S., Horn, P. J. & Peterson, C. L. SWI/SNF is required for transcriptional memory at the yeast GAL gene cluster. *Genes Dev* **21**, 997-1004, doi:10.1101/gad.1506607 (2007).
37 Booth, L. N. & Brunet, A. The aging epigenome. *Molecular cell* **62**, 728-744 (2016).
38 Oki, S. *et al.* Ch IP-Atlas: a data-mining suite powered by full integration of public Ch IP-seq data. *EMBO reports* **19**, e46255 (2018).

39 Matilainen, O., Sleiman, M. S. B., Quiros, P. M., Garcia, S. M. & Auwerx, J. The chromatin remodeling factor ISW-1 integrates organismal responses against nuclear and mitochondrial stress. *Nature communications* **8**, 1-11 (2017).

40 Riedel, C. G. *et al.* DAF-16 employs the chromatin remodeller SWI/SNF to promote stress resistance and longevity. *Nature cell biology* **15**, 491-501 (2013).

41 Zhou, L., He, B., Deng, J., Pang, S. & Tang, H. Histone acetylation promotes long-lasting defense responses and longevity following early life heat stress. *PLoS genetics* **15**, e1008122 (2019).

42 Zeng, X. *et al.* Genome-wide RNAi screen identifies networks involved in intestinal stem cell regulation in Drosophila. *Cell reports* **10**, 1226-1238 (2015).

43 Doiguchi, M. *et al.* SMARCAD1 is an ATP-dependent stimulator of nucleosomal H2A acetylation via CBP, resulting in transcriptional regulation. *Scientific reports* **6**, 1-13 (2016).

44 van der Heide, L. P. & Smidt, M. P. Regulation of FoxO activity by CBP/p300-mediated acetylation. *Trends in biochemical sciences* **30**, 81-86 (2005).

45 Martin, E., Heidari, R., Monnier, V. & Tricoire, H. Genetic Screen in Adult Drosophila Reveals That dCBP Depletion in Glial Cells Mitigates Huntington Disease Pathology through a Foxo-Dependent Pathway. *International journal of molecular sciences* **22**, 3884 (2021).

46 Liu, L.-P., Ni, J.-Q., Shi, Y.-D., Oakeley, E. J. & Sun, F.-L. Sex-specific role of Drosophila melanogaster HP1 in regulating chromatin structure and gene transcription. *Nature genetics* **37**, 1361-1366 (2005).

47 Tyagi, M., Imam, N., Verma, K. & Patel, A. K. Chromatin remodelers: We are the drivers!! *Nucleus* **7**, 388-404 (2016).

48 Wang, S. *et al.* Target analysis by integration of transcriptome and ChIP-seq data with BETA. *Nature protocols* **8**, 2502-2515 (2013).

49 Ma, Z. *et al.* Epigenetic drift of H3K27me3 in aging links glycolysis to healthy longevity in Drosophila. *Elife* **7**, e35368 (2018).

50 Acosta-Alvear, D. *et al.* XBP1 controls diverse cell type-and condition-specific transcriptional regulatory networks. *Molecular cell* **27**, 53-66 (2007).

51 Yoshida, H., Matsui, T., Yamamoto, A., Okada, T. & Mori, K. XBP1 mRNA is induced by ATF6 and spliced by IRE1 in response to ER stress to produce a highly active transcription factor. *Cell* **107**, 881-891 (2001).

52 Shen, X. *et al.* Complementary signaling pathways regulate the unfolded protein response and are required for C. elegans development. *Cell* **107**, 893-903 (2001).

53 Calfon, M. *et al.* IRE1 couples endoplasmic reticulum load to secretory capacity by processing the XBP-1 mRNA. *Nature* **415**, 92-96 (2002).

54 Ryoo, H. D., Domingos, P. M., Kang, M. J. & Steller, H. Unfolded protein response in a Drosophila model for retinal degeneration. *The EMBO journal* **26**, 242-252 (2007).

55 Huang, S., Xing, Y. & Liu, Y. Emerging roles for the ER stress sensor IRE1α in metabolic regulation and disease. *Journal of Biological Chemistry* **294**, 18726-18741 (2019).

56 Xu, T. *et al.* The IRE1α-XBP1 pathway regulates metabolic stress-induced compensatory proliferation of pancreatic β-cells. *Cell research* **24**, 1137-1140 (2014).

57 Huang, H.-W., Zeng, X., Rhim, T., Ron, D. & Ryoo, H. D. The requirement of IRE1 and XBP1 in resolving physiological stress during Drosophila development. *Journal of cell science* **130**, 3040-3049 (2017).

58 Surani, M. Glycoprotein synthesis and inhibition of protein glycosylation by tunicamycin in preimplantation embryos: influence on compaction and trophoblast adhesion. *Cell* **18**, 217 (1979).

59 Taylor, R. C. & Dillin, A. XBP-1 is a cell-nonautonomous regulator of stress resistance and longevity. *Cell* **153**, 1435-1447 (2013).

60 Wang, L., Ryoo, H. D., Qi, Y. & Jasper, H. PERK limits Drosophila lifespan by promoting intestinal stem cell proliferation in response to ER stress. *PLoS genetics* **11**, e1005220 (2015).

61 Imanikia, S., Sheng, M., Castro, C., Griffin, J. L. & Taylor, R. C. XBP-1 remodels lipid metabolism to extend longevity. *Cell reports* **28**, 581-589. e584 (2019).

62 Benayoun, B. A., Pollina, E. A. & Brunet, A. Epigenetic regulation of ageing: linking environmental inputs to genomic stability. *Nat Rev Mol Cell Biol* **16**, 593-610, doi:10.1038/nrm4048 (2015).

63 Weigelt, C. M. *et al.* An Insulin-Sensitive Circular RNA that Regulates Lifespan in Drosophila. *Molecular cell* **79**, 268-279. e265 (2020).

64 Harris, S. E. *et al.* Age-related gene expression changes, and transcriptome wide association study of physical and cognitive aging traits, in the Lothian Birth Cohort 1936. *Aging (Albany NY)* **9**, 2489 (2017).

65 Schaum, N. *et al.* Ageing hallmarks exhibit organ-specific temporal signatures. *Nature* **583**, 596-602 (2020).

66 Hou, Z. & Fuiman, L. A. Nutritional programming in fishes: insights from mammalian studies. *Reviews in Fish Biology and Fisheries* **30**, 67-92 (2020).

67 Shimazu, T. *et al.* Suppression of oxidative stress by β-hydroxybutyrate, an endogenous histone deacetylase inhibitor. *Science* **339**, 211-214 (2013).

68 Zhang, W., Qu, J., Liu, G.-H. & Belmonte, J. C. I. The ageing epigenome and its rejuvenation. *Nature reviews Molecular cell biology* **21**, 137-150 (2020).

69 Yan, Y. *et al.* HDAC6 suppresses age-dependent ectopic fat accumulation by maintaining the proteostasis of PLIN2 in Drosophila. *Developmental cell* **43**, 99-111. e115 (2017).

70 Peleg, S. *et al.* Life span extension by targeting a link between metabolism and histone acetylation in Drosophila. *EMBO reports* **17**, 455-469 (2016).

71 Lu, Y.-X. *et al.* A TORC1-histone axis regulates chromatin organisation and non-canonical induction of autophagy to ameliorate ageing. *Elife* **10**, e62233 (2021).

72 Brown, A. K., Maybury-Lewis, S. Y. & Webb, A. E. Integrative multi-omics analysis reveals conserved hierarchical mechanisms of FOXO3 pioneer-factor activity. *bioRxiv* (2021).

73 Hatta, M. & Cirillo, L. A. Chromatin opening and stable perturbation of core histone: DNA contacts by FoxO1. *Journal of Biological Chemistry* **282**, 35583-35593 (2007).

74 Iwafuchi-Doi, M. *et al.* The pioneer transcription factor FoxA maintains an accessible nucleosome configuration at enhancers for tissue-specific gene activation. *Molecular cell* **62**, 79-91 (2016).

75 Lee, S. & Dong, H. H. FoxO integration of insulin signaling with glucose and lipid metabolism. *The Journal of endocrinology* **233**, R67 (2017).

76 Zhao, P. *et al.* Fat body Ire1 regulates lipid homeostasis through the Xbp1s-FoxO axis in Drosophila. *Iscience* **24**, 102819 (2021).

77 Imanikia, S., Özbey, N. P., Krueger, C., Casanueva, M. O. & Taylor, R. C. Neuronal XBP-1 activates intestinal lysosomes to improve proteostasis in C. elegans. *Current Biology* **29**, 2322-2338. e2327 (2019).
78 Wang, Z. V. *et al.* Spliced X-box binding protein 1 couples the unfolded protein response to hexosamine biosynthetic pathway. *Cell* **156**, 1179-1192 (2014).
79 van der Harg, J. M. *et al.* The UPR reduces glucose metabolism via IRE1 signaling. *Biochimica et Biophysica Acta (BBA)-Molecular Cell Research* **1864**, 655-665 (2017).
80 Lu, Y. *et al.* Reprogramming to recover youthful epigenetic information and restore vision. *Nature* **588**, 124-129 (2020).
81 Bass, T. M. *et al.* Optimization of dietary restriction protocols in Drosophila. *The Journals of Gerontology Series A: Biological Sciences and Medical Sciences* **62**, 1071-1081 (2007).
82 Larkin, A. *et al.* FlyBase: updates to the Drosophila melanogaster knowledge base. *Nucleic acids research* **49**, D899-D907 (2021).
83 Piper, M. D. & Partridge, L. Protocols to study aging in Drosophila. *Drosophila*, 291-302 (2016).
84 Clancy, D. & Kennington, W. A simple method to achieve consistent larval density in bottle cultures. *Drosophila Information Service* **84**, 168-169 (2001).
85 Corrales, G. M. *et al.* Partial inhibition of RNA polymerase I promotes animal health and longevity. *Cell reports* **30**, 1661-1669. e1664 (2020).
86 Schindelin, J. *et al.* Fiji: an open-source platform for biological-image analysis. *Nature methods* **9**, 676-682 (2012).
87 Bateman, J. R., Lee, A. M. & Wu, C.-T. Site-specific transformation of Drosophila via ϕC31 integrase-mediated cassette exchange. *Genetics* **173**, 769-777 (2006).
88 Buenrostro, J. D., Wu, B., Chang, H. Y. & Greenleaf, W. J. ATAC-seq: a method for assaying chromatin accessibility genome-wide. *Current protocols in molecular biology* **109**, 21.29. 21-21.29. 29 (2015).
89 Picelli, S. *et al.* Tn5 transposase and tagmentation procedures for massively scaled sequencing projects. *Genome research* **24**, 2033-2040 (2014).
90 Alexa, A. & Rahnenführer, J. Gene set enrichment analysis with topGO. *Bioconductor Improv* **27**, 1-26 (2009).
91 Huang, D. W., Sherman, B. T. & Lempicki, R. A. Bioinformatics enrichment tools: paths toward the comprehensive functional analysis of large gene lists. *Nucleic acids research* **37**, 1-13 (2009).
92 Gu, Z., Gu, L., Eils, R., Schlesner, M. & Brors, B. circlize implements and enhances circular visualization in R. *Bioinformatics* **30**, 2811-2812 (2014).
93 Yu, G., Wang, L.-G. & He, Q.-Y. ChIPseeker: an R/Bioconductor package for ChIP peak annotation, comparison and visualization. *Bioinformatics* **31**, 2382-2383 (2015).
94 Gel, B. *et al.* regioneR: an R/Bioconductor package for the association analysis of genomic regions based on permutation tests. *Bioinformatics* **32**, 289-291 (2016).
95 Viechtbauer, W. Conducting meta-analyses in R with the metafor package. *Journal of statistical software* **36**, 1-48 (2010).
96 Aibar, S. *et al.* SCENIC: single-cell regulatory network inference and clustering. *Nature methods* **14**, 1083-1086 (2017).
97 Villanueva, M. *et al.* Sensory deprivation in Staphylococcus aureus. *Nature communications* **9**, 1-12 (2018).

98 Pang, Z. *et al.* MetaboAnalyst 5.0: narrowing the gap between raw spectra and functional insights. *Nucleic acids research* (2021).
99 Haug, K. *et al.* MetaboLights: a resource evolving in response to the needs of its scientific community. *Nucleic acids research* **48**, D440-D444 (2020).
100 Juricic, P. *et al.* Long-lasting geroprotection from brief rapamycin treatment in early adulthood by persistently increased intestinal autophagy. *Nature Aging*, 1-13 (2022).

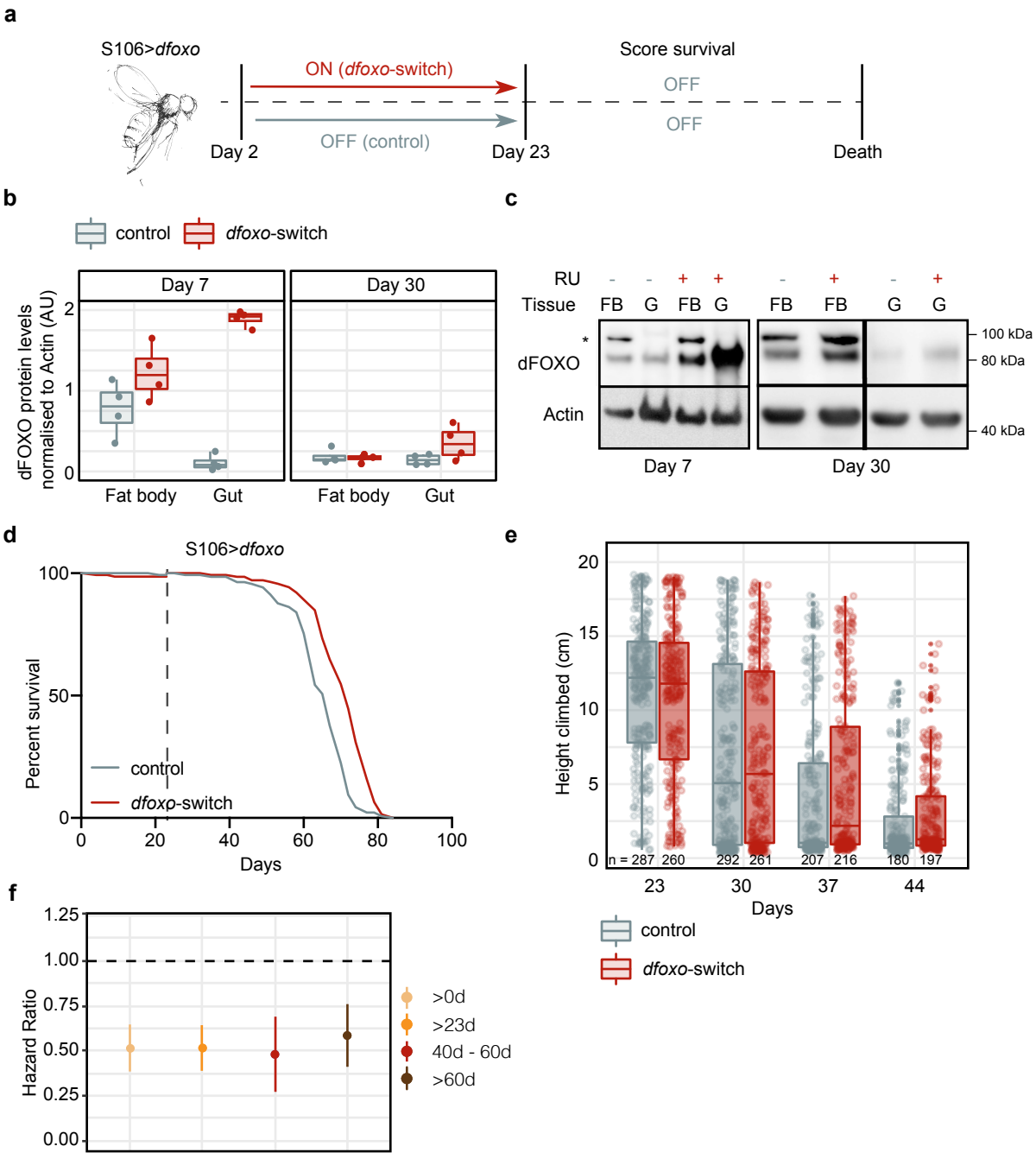
a
S106>dfoxo
ON (dfoxo-switch)
OFF (control)
Score survival
OFF
OFF
Day 2
Day 23
Death
b
control
dfoxo-switch
Day 7
Day 30
dFOXO protein levels normalised to Actin (AU)
Fat body
Gut
Fat body
Gut
c
RU
Tissue
FB G FB G FB FB G G
dFOXO
Actin
100 kDa
80 kDa
40 kDa
Day 7
Day 30
d
S106>dfoxo
Percent survival
control
dfoxo-switch
Days
e
Height climbed (cm)
n = 287 260 292 261 207 216 180 197
Days
control
dfoxo-switch
f
Hazard Ratio
>0d
>23d
40d - 60d
>60d

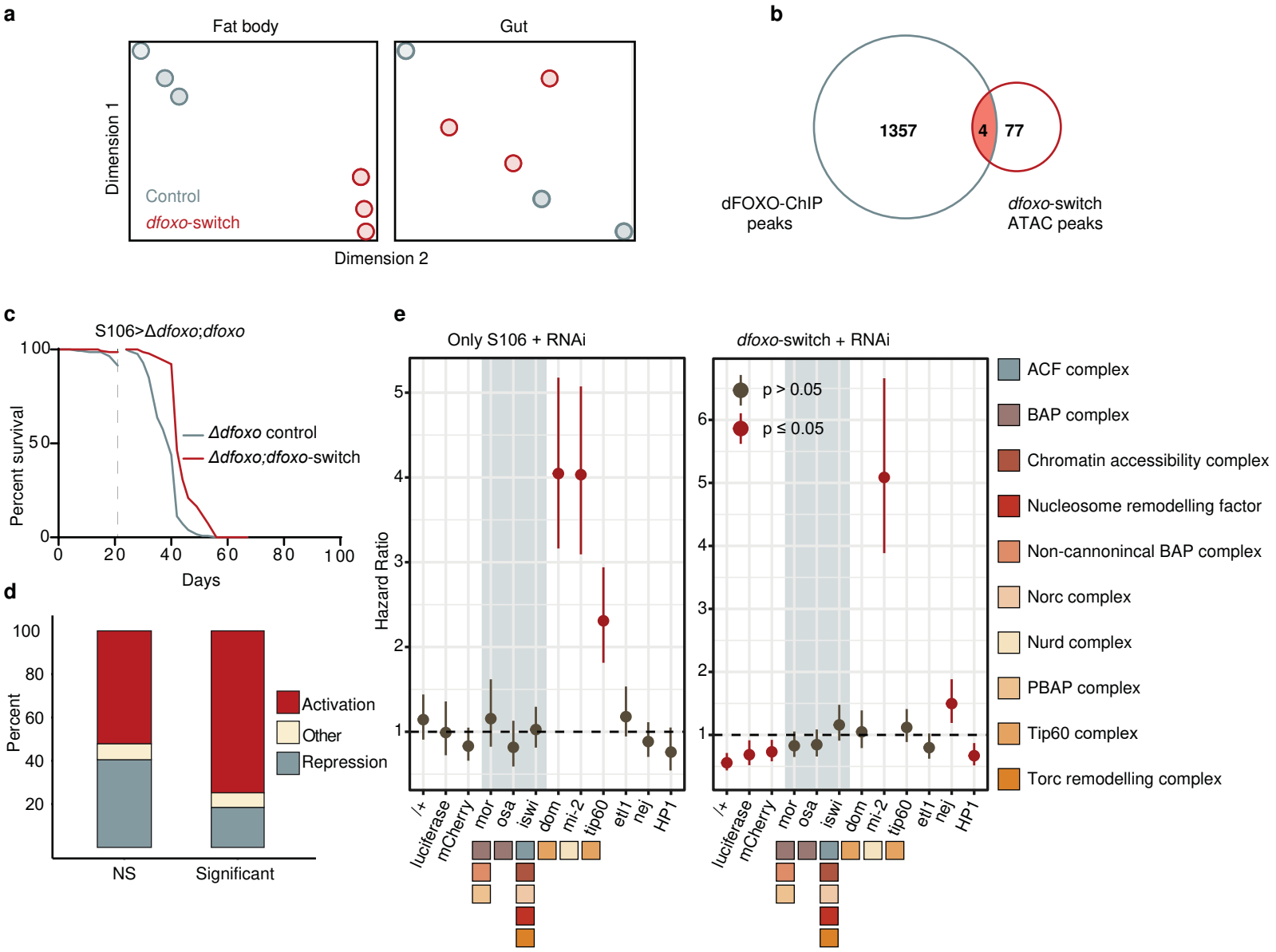
a
Fat body
Gut
Dimension 1
Dimension 2
Control
dfoxo-switch
b
1357
4
77
dFOXO-ChIP peaks
dfoxo-switch ATAC peaks
c
S106>Δdfoxo;dfoxo
Percent survival
Days
Δdfoxo control
Δdfoxo;dfoxo-switch
d
Percent
Activation
Other
Repression
NS
Significant
e
Only S106 + RNAi
dfoxo-switch + RNAi
Hazard Ratio
p > 0.05
p ≤ 0.05
/+
luciferase
mCherry
mor
osa
iswi
dom
mi-2
tip60
etl1
nej
HP1
ACF complex
BAP complex
Chromatin accessibility complex
Nucleosome remodelling factor
Non-cannonincal BAP complex
Norc complex
Nurd complex
PBAP complex
Tip60 complex
Torc remodelling complex

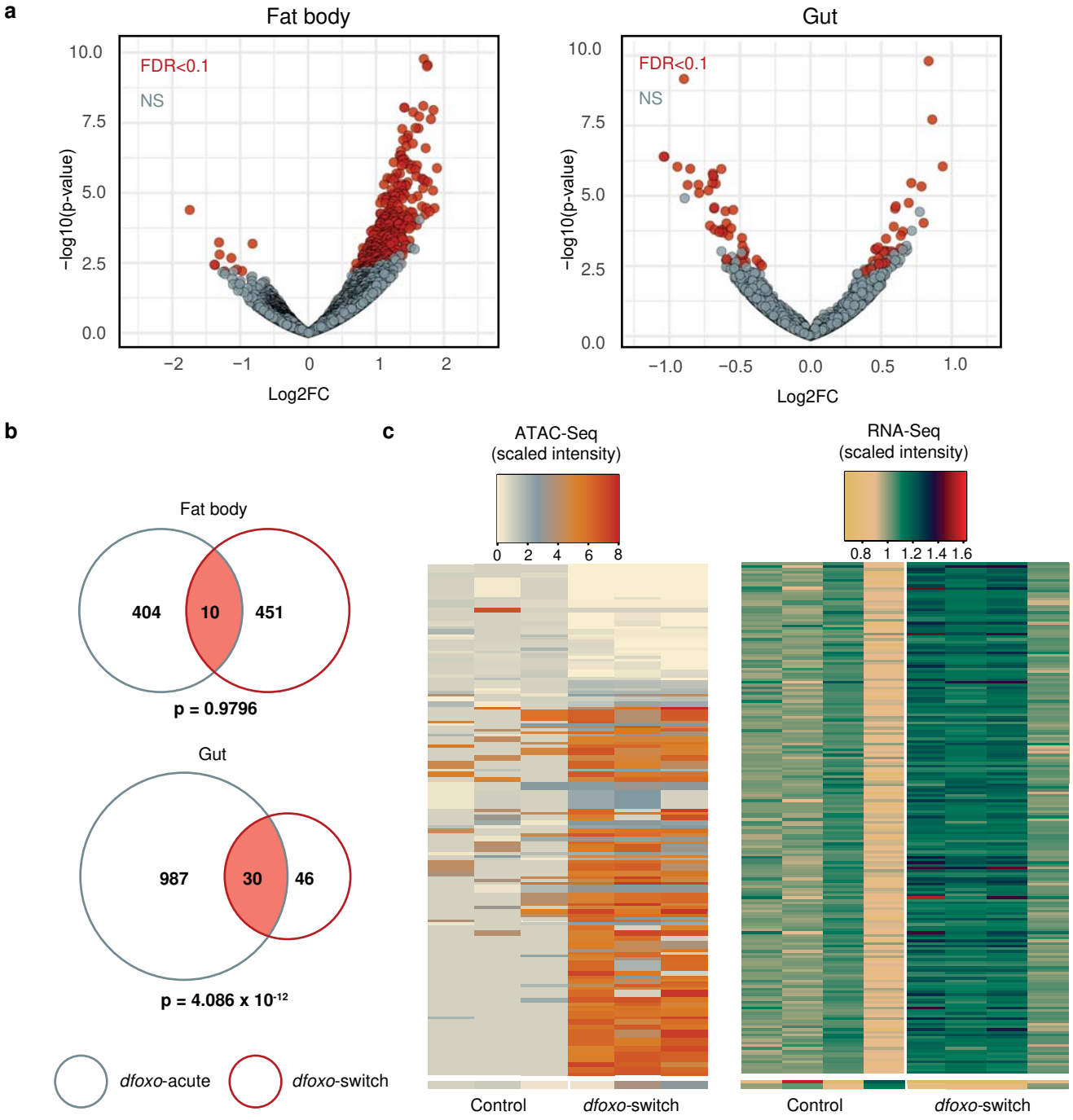
a
Fat body
Gut
FDR<0.1
NS
−log10(p-value)
Log2FC
b
Fat body
404
10
451
p = 0.9796
Gut
987
30
46
p = 4.086 x 10-12
dfoxo-acute
dfoxo-switch
c
ATAC-Seq
(scaled intensity)
RNA-Seq
(scaled intensity)
Control
dfoxo-switch

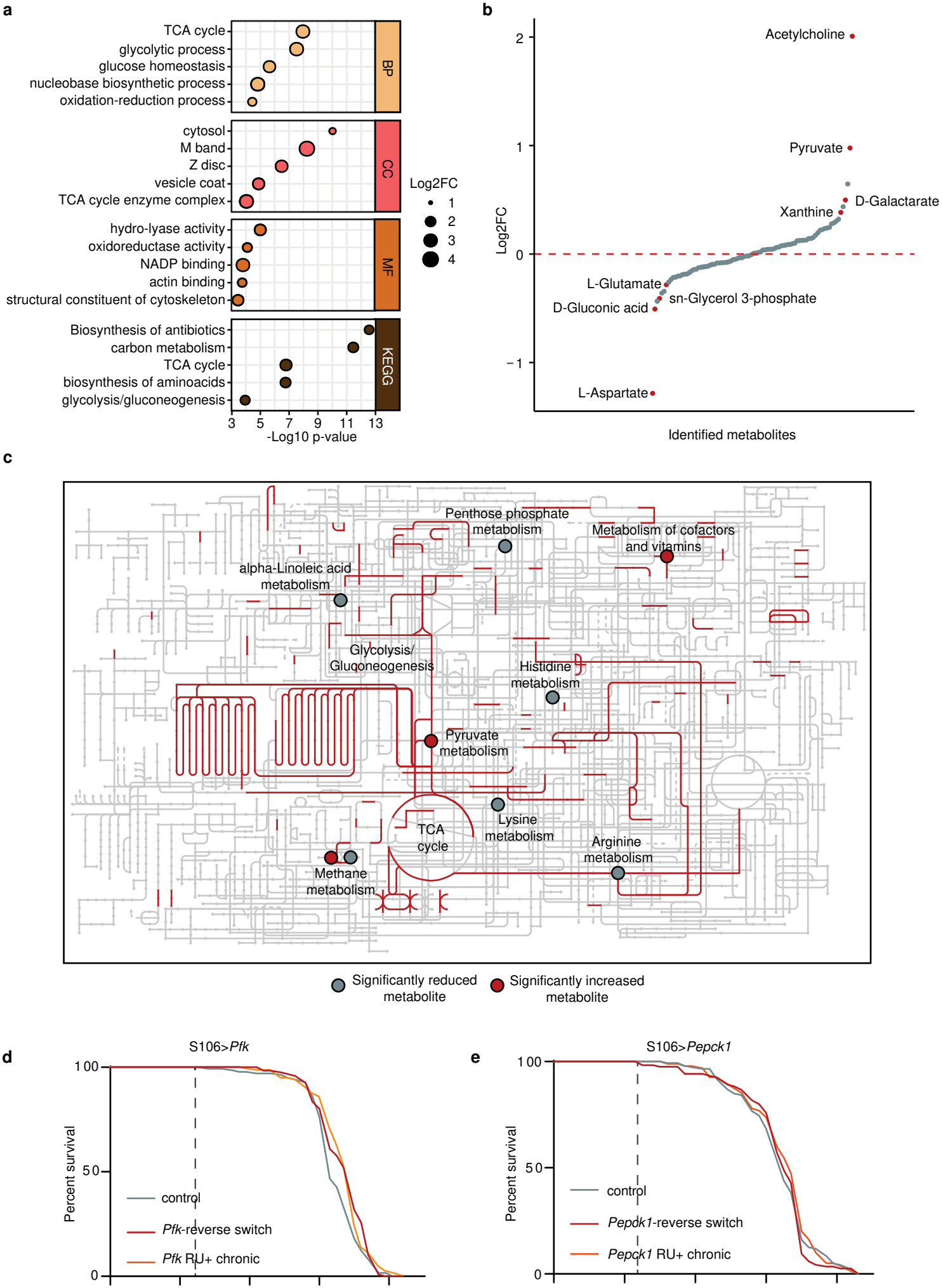
a
TCA cycle
glycolytic process
glucose homeostasis
nucleobase biosynthetic process
oxidation-reduction process
BP
cytosol
M band
Z disc
vesicle coat
TCA cycle enzyme complex
CC
hydro-lyase activity
oxidoreductase activity
NADP binding
actin binding
structural constituent of cytoskeleton
MF
Biosynthesis of antibiotics
carbon metabolism
TCA cycle
biosynthesis of aminoacids
glycolysis/gluconeogenesis
KEGG
3 5 7 9 11 13
-Log10 p-value
Log2FC
1
2
3
4
b
Acetylcholine
Pyruvate
D-Galactarate
Xanthine
L-Glutamate
sn-Glycerol 3-phosphate
D-Gluconic acid
L-Aspartate
Log2FC
2
1
0
−1
Identified metabolites
c
Penthose phosphate metabolism
Metabolism of cofactors and vitamins
alpha-Linoleic acid metabolism
Glycolysis/ Gluconeogenesis
Histidine metabolism
Pyruvate metabolism
TCA cycle
Lysine metabolism
Arginine metabolism
Methane metabolism
Significantly reduced metabolite
Significantly increased metabolite
d
S106>Pfk
Percent survival
100
50
0
control
Pfk-reverse switch
Pfk RU+ chronic
0 20 40 60 80
Days
e
S106>Pepck1
Percent survival
100
50
0
control
Pepdk1-reverse switch
Pepck1 RU+ chronic
0 20 40 60 80
Days

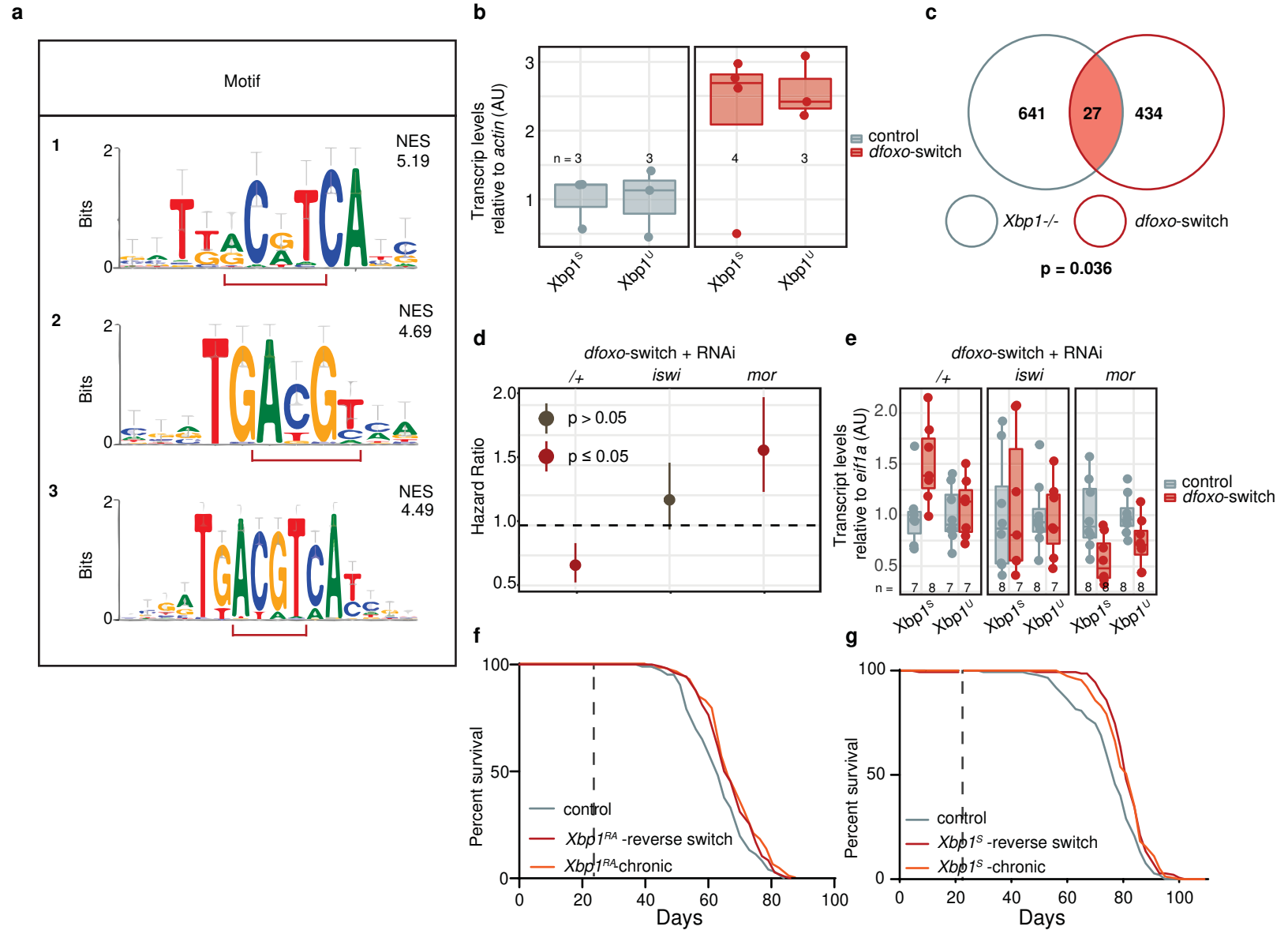
a
Motif
1
NES
5.19
Bits
2
0
2
NES
4.69
Bits
2
0
3
NES
4.49
Bits
2
0
b
Transcrip levels
relative to actin (AU)
3
2
1
n = 3
3
4
3
control
dfoxo-switch
Xbp1S
Xbp1U
Xbp1S
Xbp1U
c
641
27
434
Xbp1-/-
dfoxo-switch
p = 0.036
d
dfoxo-switch + RNAi
/+
iswi
mor
Hazard Ratio
2.0
1.5
1.0
0.5
p > 0.05
p ≤ 0.05
e
dfoxo-switch + RNAi
/+
iswi
mor
Transcript levels
relative to eif1a (AU)
2.0
1.5
1.0
0.5
n =
7 8 7 7
8 7 8 7
8 8 8 8
control
dfoxo-switch
Xbp1S
Xbp1U
Xbp1S
Xbp1U
Xbp1S
Xbp1U
f
Percent survival
100
50
0
control
Xbp1RA -reverse switch
Xbp1RA chronic
0
20
40
60
80
100
Days
g
Percent survival
100
50
0
control
Xbp1S -reverse switch
Xbp1S -chronic
0
20
40
60
80
100
Days

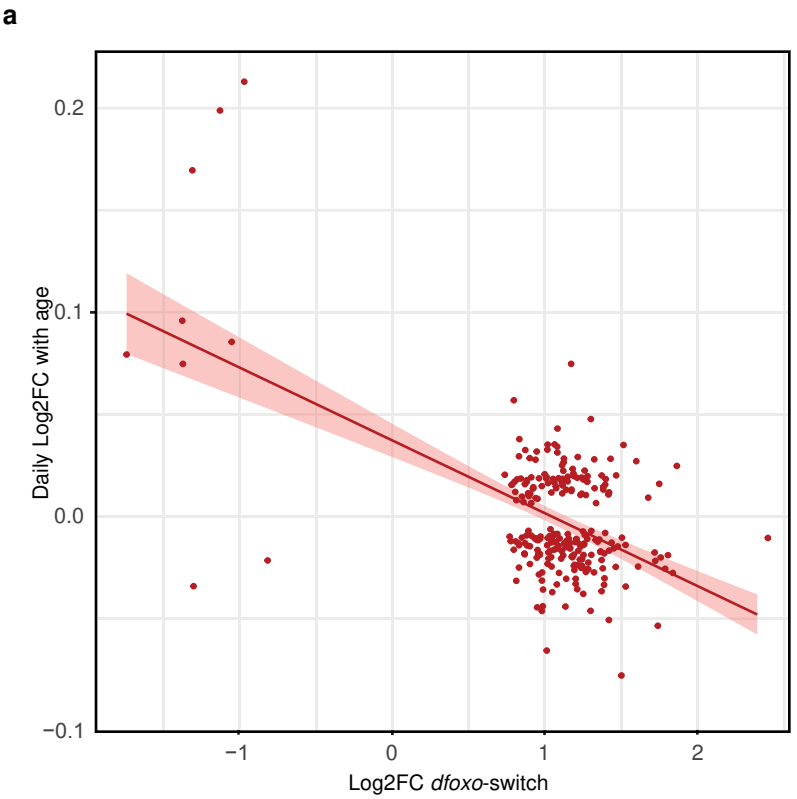
a
0.2
0.1
0.0
−0.1
Daily Log2FC with age
−1
0
1
2
Log2FC *dfoxo*-switch

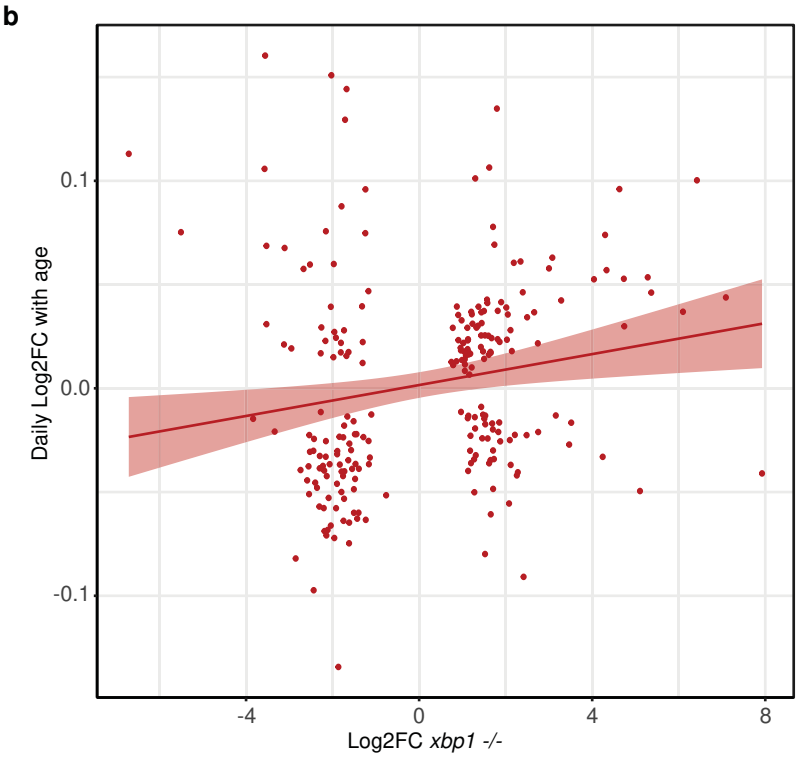
b
0.1
0.0
-0.1
Daily Log2FC with age
-4
0
4
8
Log2FC *xbp1* -/-

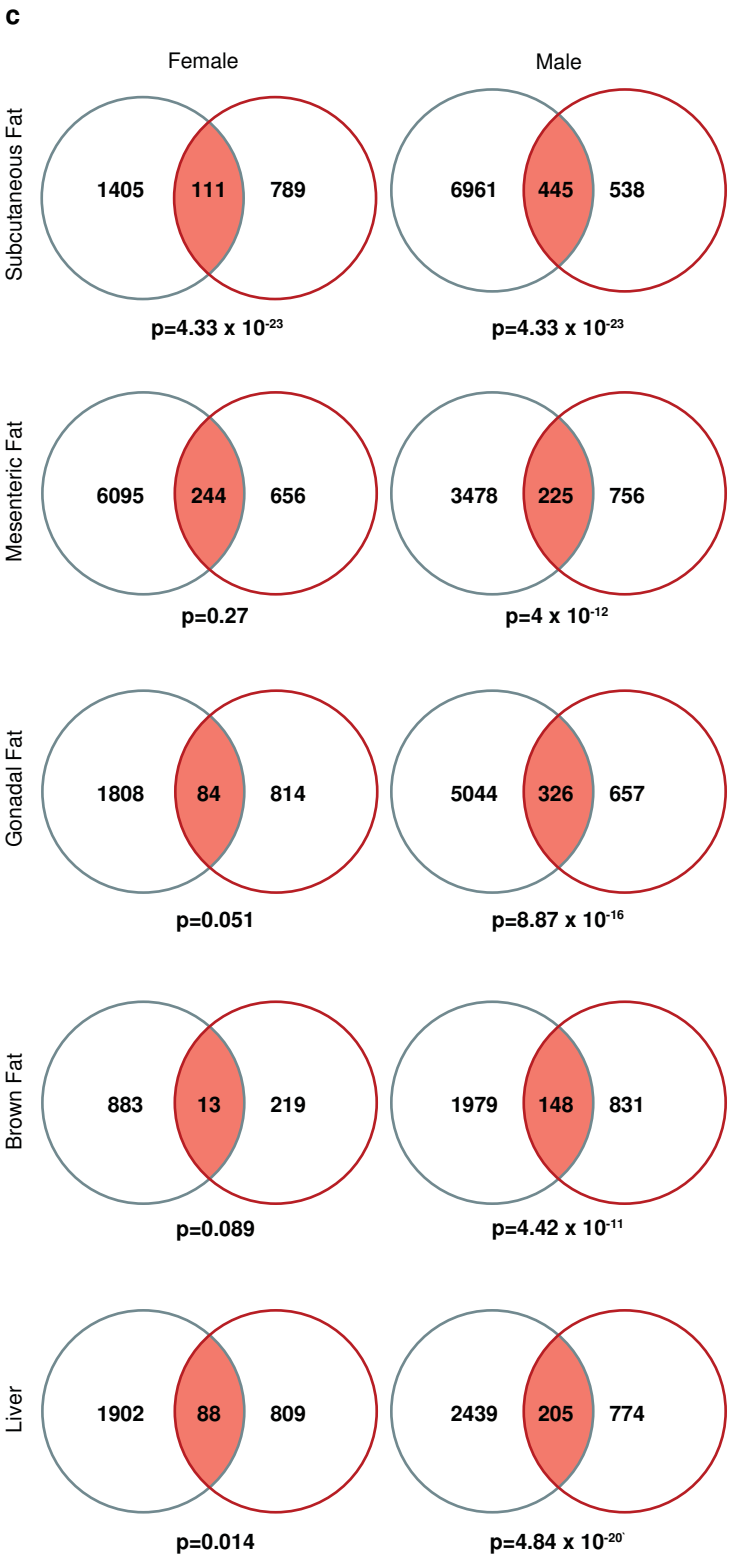
c
Female
Male
Subcutaneous Fat
1405
111
789
p=4.33 x 10-23
6961
445
538
p=4.33 x 10-23
Mesenteric Fat
6095
244
656
p=0.27
3478
225
756
p=4 x 10-12
Gonadal Fat
1808
84
814
p=0.051
5044
326
657
p=8.87 x 10-16
Brown Fat
883
13
219
p=0.089
1979
148
831
p=4.42 x 10-11
Liver
1902
88
809
p=0.014
2439
205
774
p=4.84 x 10-20

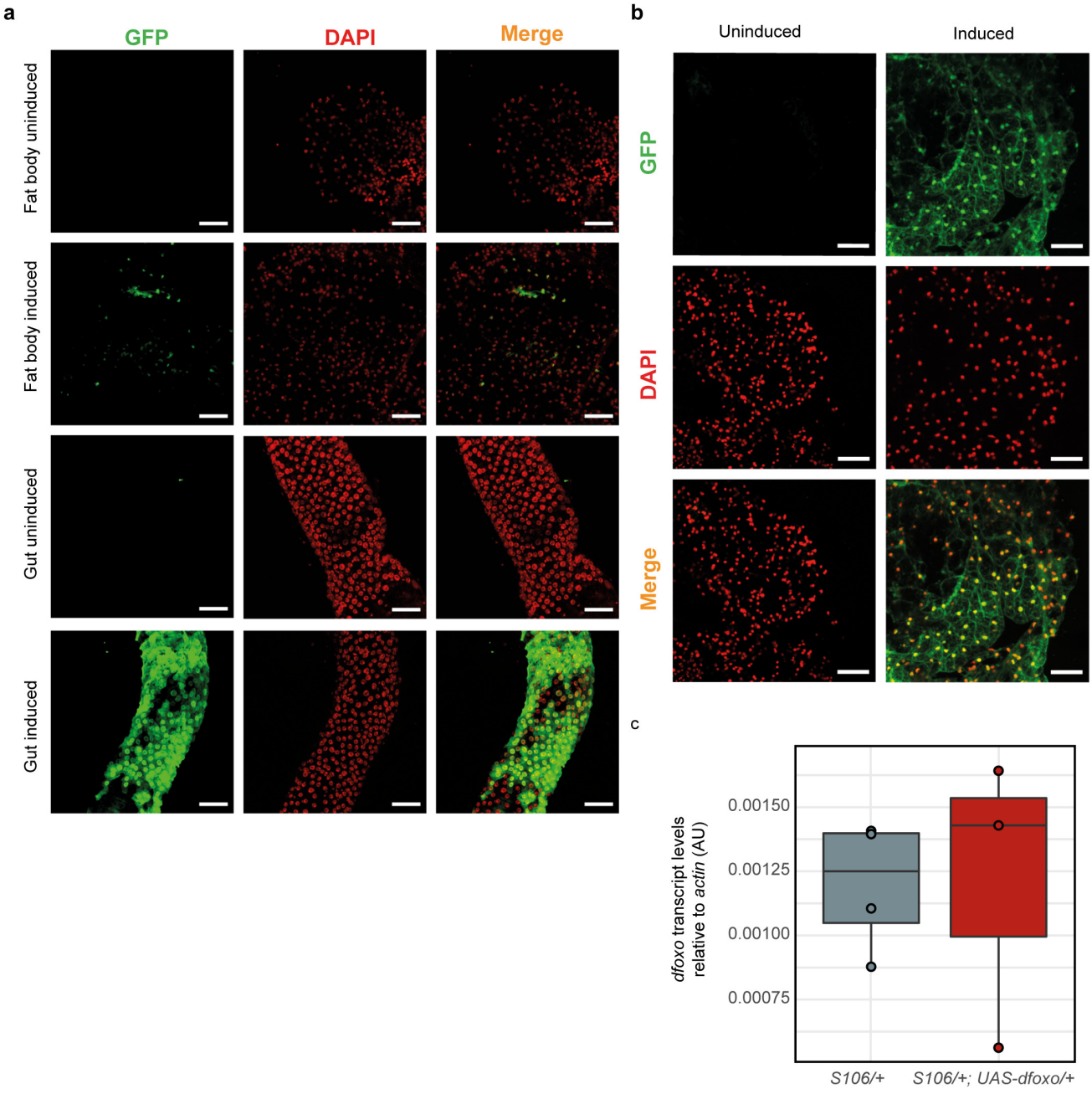
a
GFP
DAPI
Merge
Fat body uninduced
Fat body induced
Gut uninduced
Gut induced
b
Uninduced
Induced
GFP
DAPI
Merge
c
dfoxo transcript levels relative to actin (AU)
0.00150
0.00125
0.00100
0.00075
S106/+
S106/+; UAS-dfoxo/+
d
1 week old, dFOXO
RU
Tissue
FB G FB G FB G FB G FB G FB G FB G FB G
Molecular mass (kDa)
93
72
60
31
24
4 weeks old, dFOXO
G G G G G G G G FB FB FB FB FB FB FB FB
100
80
60
20
1 week old, Actin
4 weeks old, Actin
40
30

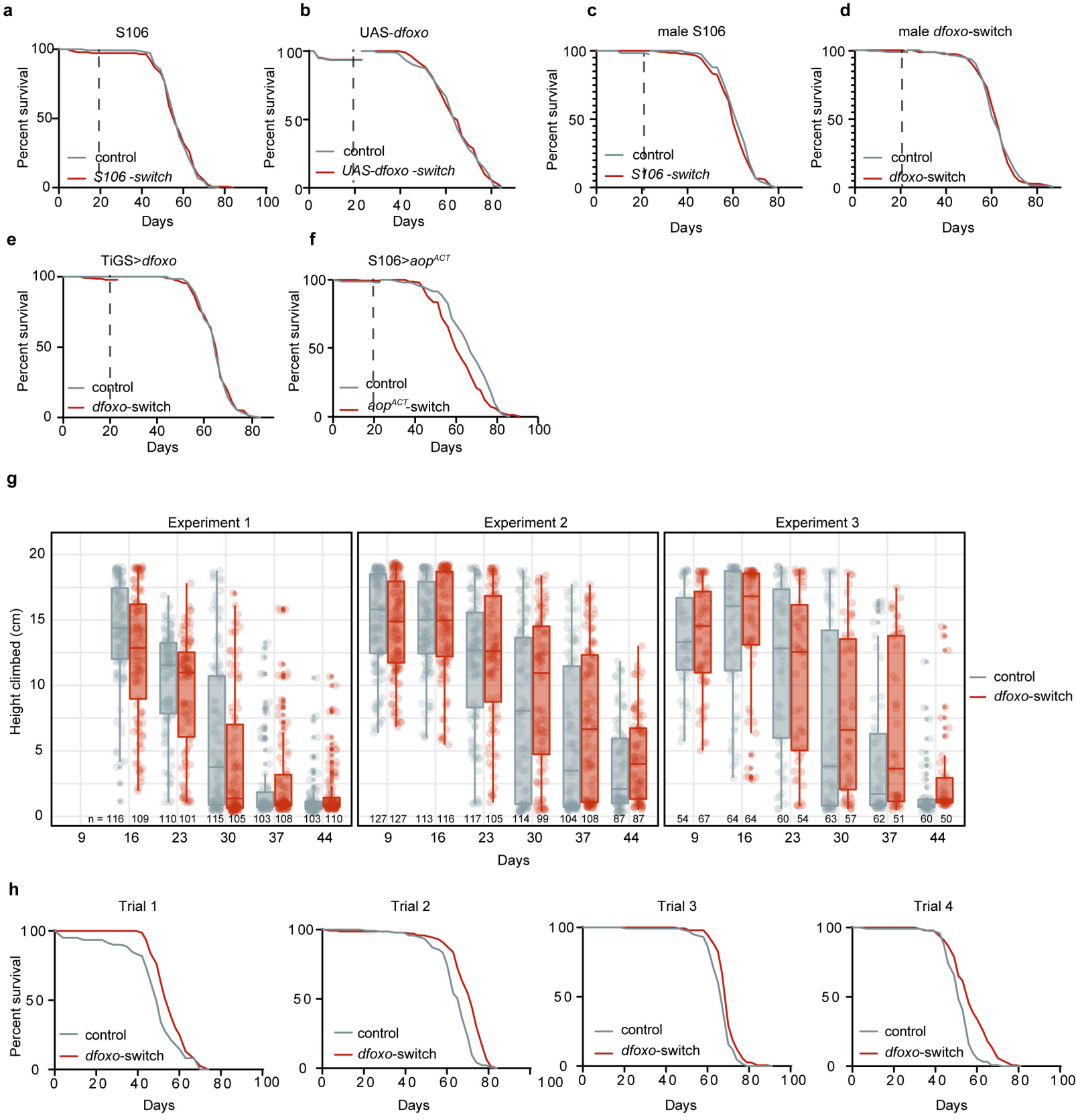
a
S106
Percent survival
Days
control
S106 -switch
b
UAS-dfoxo
control
UAS-dfoxo -switch
c
male S106
control
S106 -switch
d
male dfoxo-switch
control
dfoxo-switch
e
TiGS>dfoxo
control
dfoxo-switch
f
S106>aop^ACT
control
aop^ACT-switch
g
Experiment 1
Experiment 2
Experiment 3
Height climbed (cm)
n = 116 109 110 101 115 105 103 108 103 110
127 127 113 116 117 105 114 99 104 108 87 87
54 67 64 64 60 54 63 57 62 51 60 50
Days
control
dfoxo-switch
h
Trial 1
Trial 2
Trial 3
Trial 4
Percent survival
control
dfoxo-switch
Days

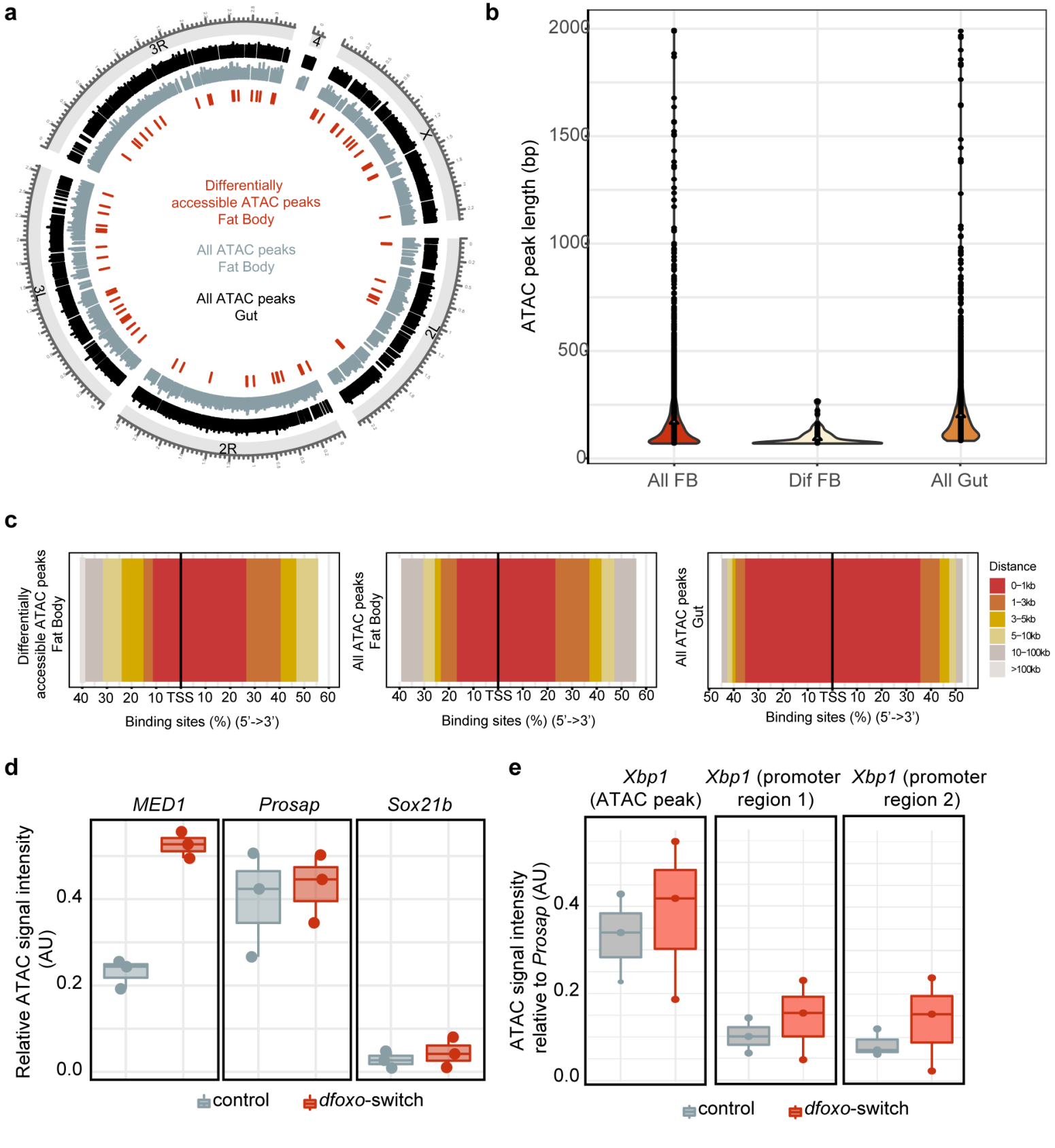
a
3R
4
X
3L
2L
2R
Differentially accessible ATAC peaks Fat Body
All ATAC peaks Fat Body
All ATAC peaks Gut
b
ATAC peak length (bp)
2000
1500
1000
500
0
All FB
Dif FB
All Gut
c
Differentially accessible ATAC peaks Fat Body
All ATAC peaks Fat Body
All ATAC peaks Gut
40 30 20 10 TSS 10 20 30 40 50 60
50 40 30 20 10 TSS 10 20 30 40 50
Binding sites (%) (5'->3')
Distance
0–1kb
1–3kb
3–5kb
5–10kb
10–100kb
>100kb
d
MED1
Prosap
Sox21b
Relative ATAC signal intensity (AU)
0.4
0.2
0.0
control
dfoxo-switch
e
Xbp1 (ATAC peak)
Xbp1 (promoter region 1)
Xbp1 (promoter region 2)
ATAC signal intensity relative to Prosap (AU)
0.4
0.2
0.0
control
dfoxo-switch

a

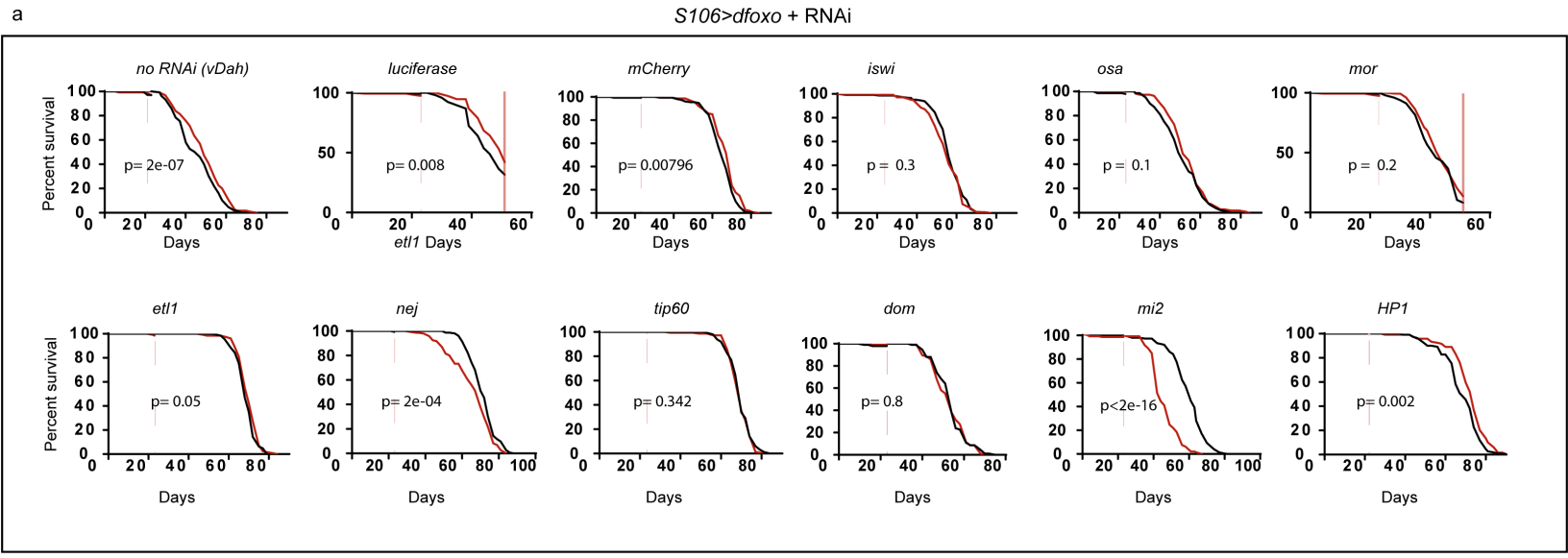
S106>dfoxo + RNAi
no RNAi (vDah)
luciferase
mCherry
iswi
osa
mor
etl1
nej
tip60
dom
mi2
HP1
Percent survival
Days
etl1 Days
p= 2e-07
p= 0.008
p= 0.00796
p = 0.3
p = 0.1
p = 0.2
p= 0.05
p= 2e-04
p= 0.342
p= 0.8
p<2e-16
p= 0.002

b

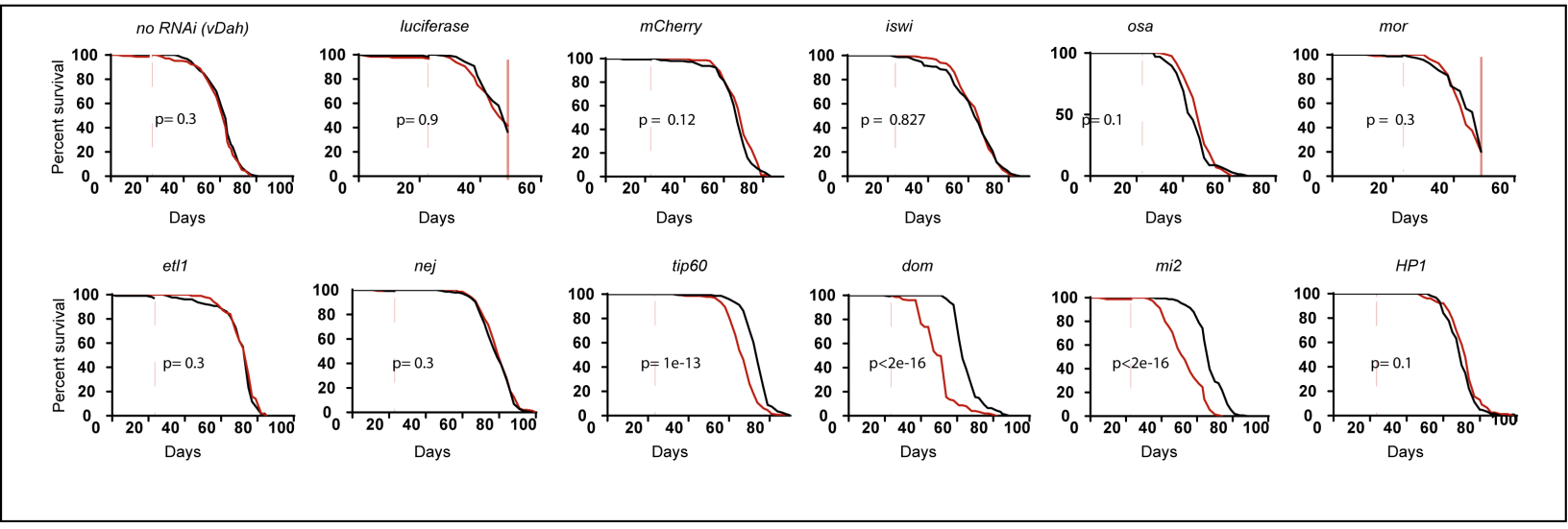
S106 + RNAi
no RNAi (vDah)
luciferase
mCherry
iswi
osa
mor
etl1
nej
tip60
dom
mi2
HP1
Percent survival
Days
p= 0.3
p= 0.9
p = 0.12
p = 0.827
p= 0.1
p = 0.3
p= 0.3
p= 0.3
p= 1e-13
p<2e-16
p<2e-16
p= 0.1

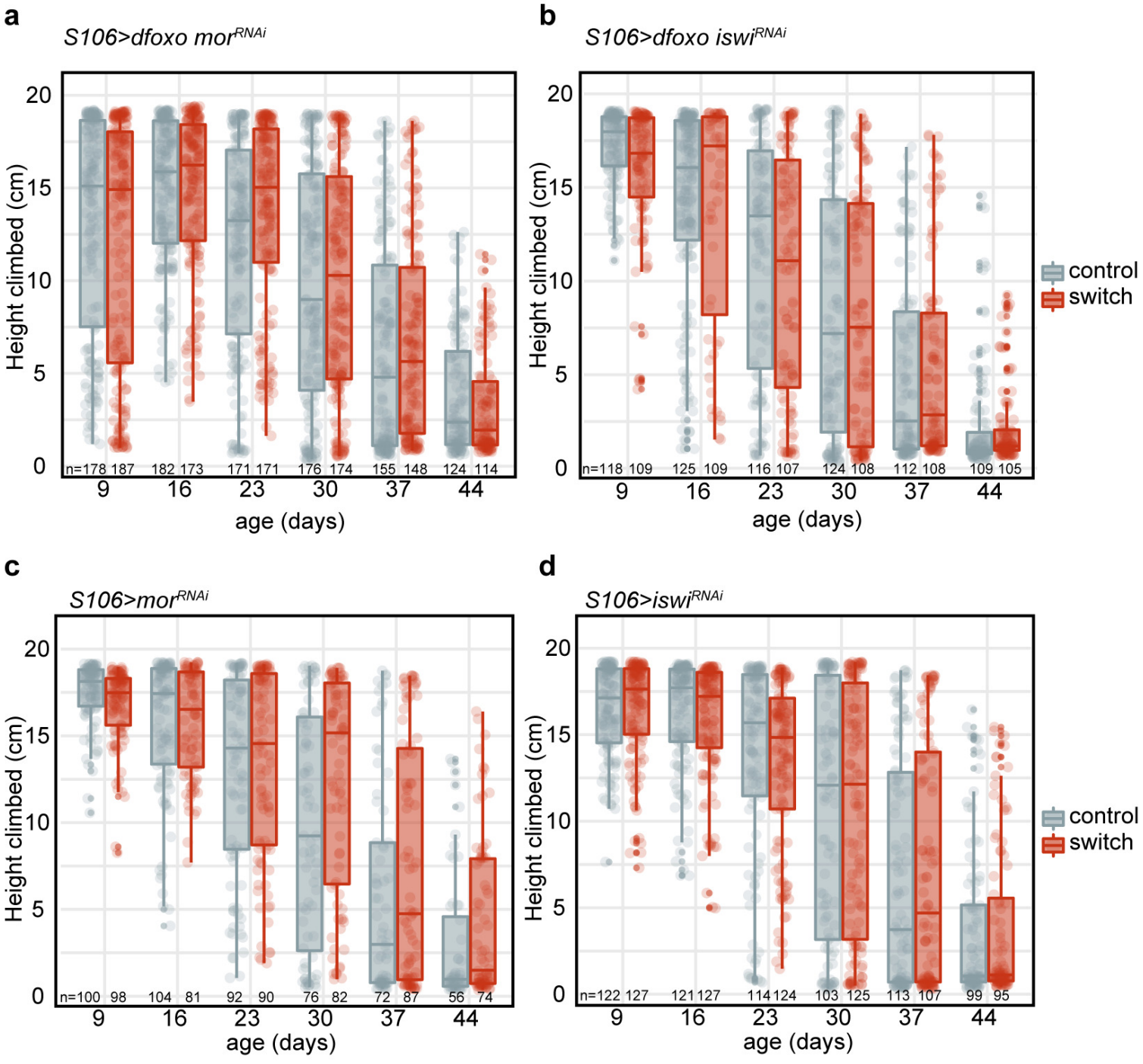
a
S106>dfoxo mor^RNAi
b
S106>dfoxo iswi^RNAi
c
S106>mor^RNAi
d
S106>iswi^RNAi
Height climbed (cm)
age (days)
control
switch
n=178 187 182 173 171 171 176 174 155 148 124 114
n=118 109 125 109 116 107 124 108 112 108 109 105
n=100 98 104 81 92 90 76 82 72 87 56 74
n=122 127 121 127 114 124 103 125 113 107 99 95

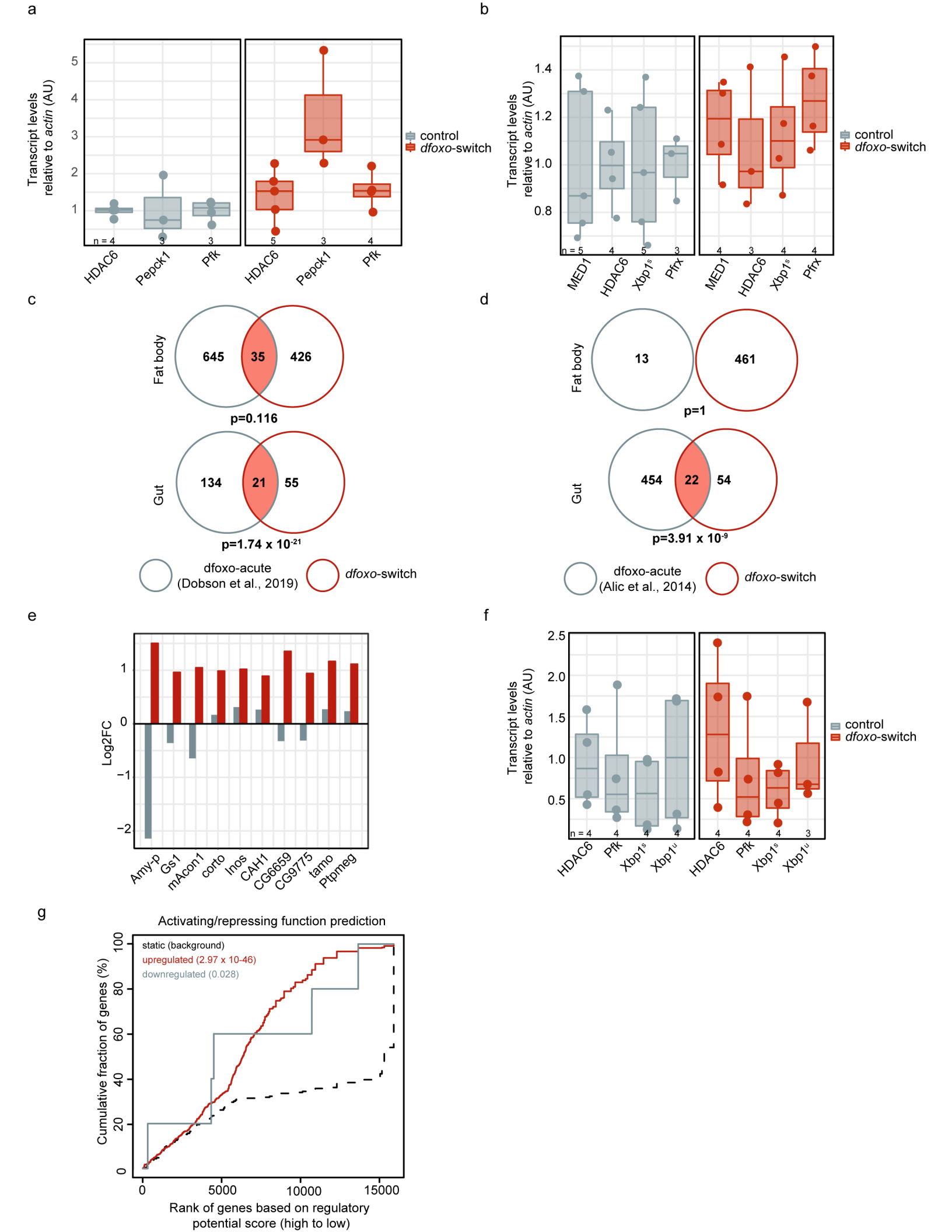
a
Transcript levels relative to actin (AU)
control
dfoxo-switch
HDAC6
Pepck1
Pfk
b
Transcript levels relative to actin (AU)
MED1
HDAC6
Xbp1s
Pfrx
c
Fat body
645
35
426
p=0.116
Gut
134
21
55
p=1.74 x 10-21
dfoxo-acute (Dobson et al., 2019)
dfoxo-switch
d
Fat body
13
461
p=1
Gut
454
22
54
p=3.91 x 10-9
dfoxo-acute (Alic et al., 2014)
dfoxo-switch
e
Log2FC
Amy-p
Gs1
mAcon1
corto
Inos
CAH1
CG6659
CG9775
tamo
Ptpmeg
f
Transcript levels relative to actin (AU)
HDAC6
Pfk
Xbp1s
Xbp1u
g
Activating/repressing function prediction
static (background)
upregulated (2.97 x 10-46)
downregulated (0.028)
Cumulative fraction of genes (%)
Rank of genes based on regulatory potential score (high to low)

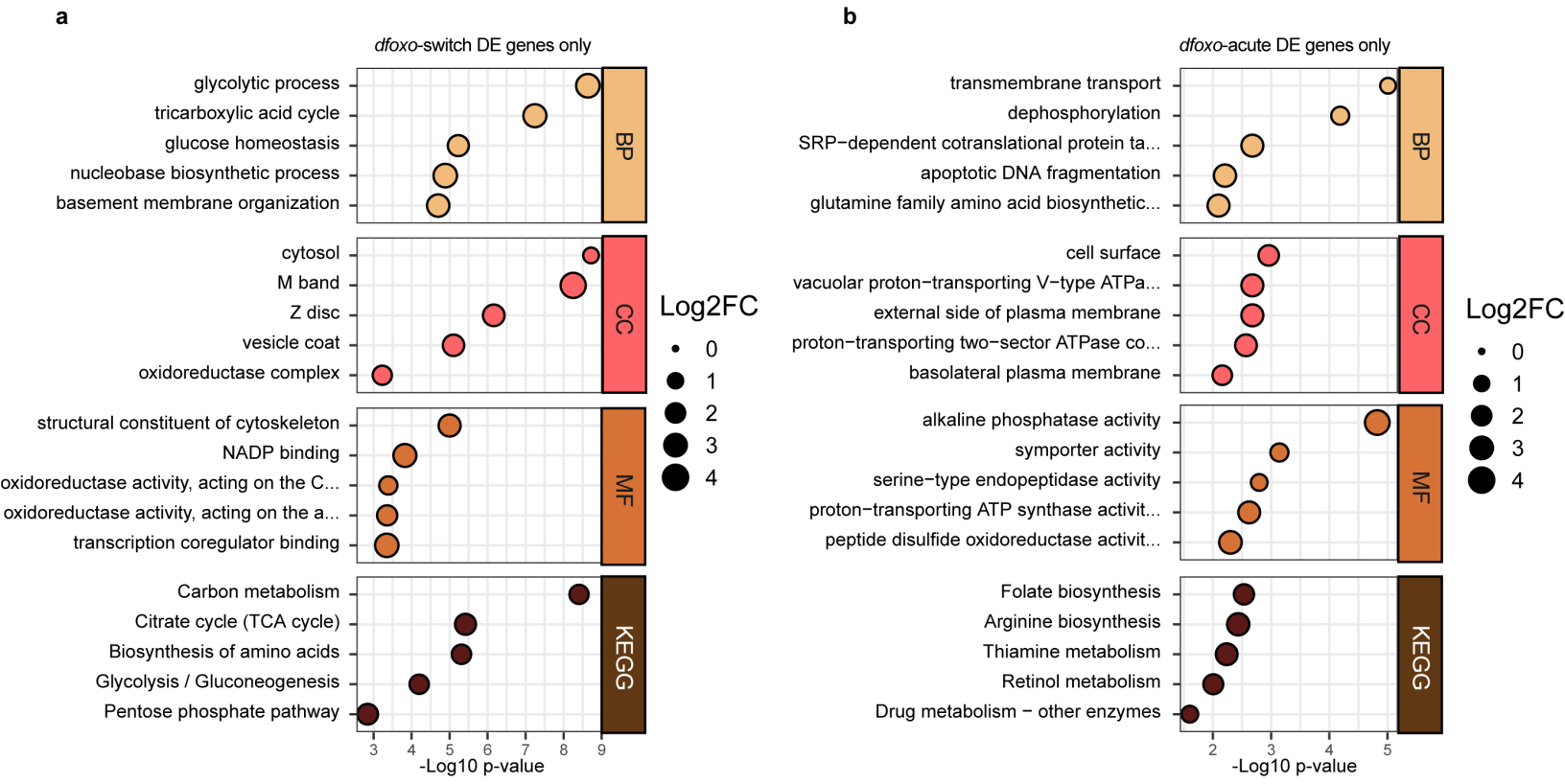
a
dfoxo-switch DE genes only
glycolytic process
tricarboxylic acid cycle
glucose homeostasis
nucleobase biosynthetic process
basement membrane organization
BP
cytosol
M band
Z disc
vesicle coat
oxidoreductase complex
CC
structural constituent of cytoskeleton
NADP binding
oxidoreductase activity, acting on the C...
oxidoreductase activity, acting on the a...
transcription coregulator binding
MF
Carbon metabolism
Citrate cycle (TCA cycle)
Biosynthesis of amino acids
Glycolysis / Gluconeogenesis
Pentose phosphate pathway
KEGG
3 4 5 6 7 8 9
-Log10 p-value
Log2FC
0
1
2
3
4
b
dfoxo-acute DE genes only
transmembrane transport
dephosphorylation
SRP−dependent cotranslational protein ta...
apoptotic DNA fragmentation
glutamine family amino acid biosynthetic...
BP
cell surface
vacuolar proton−transporting V−type ATPa...
external side of plasma membrane
proton−transporting two−sector ATPase co...
basolateral plasma membrane
CC
alkaline phosphatase activity
symporter activity
serine−type endopeptidase activity
proton−transporting ATP synthase activit...
peptide disulfide oxidoreductase activit...
MF
Folate biosynthesis
Arginine biosynthesis
Thiamine metabolism
Retinol metabolism
Drug metabolism − other enzymes
KEGG
2 3 4 5
-Log10 p-value
Log2FC
0
1
2
3
4

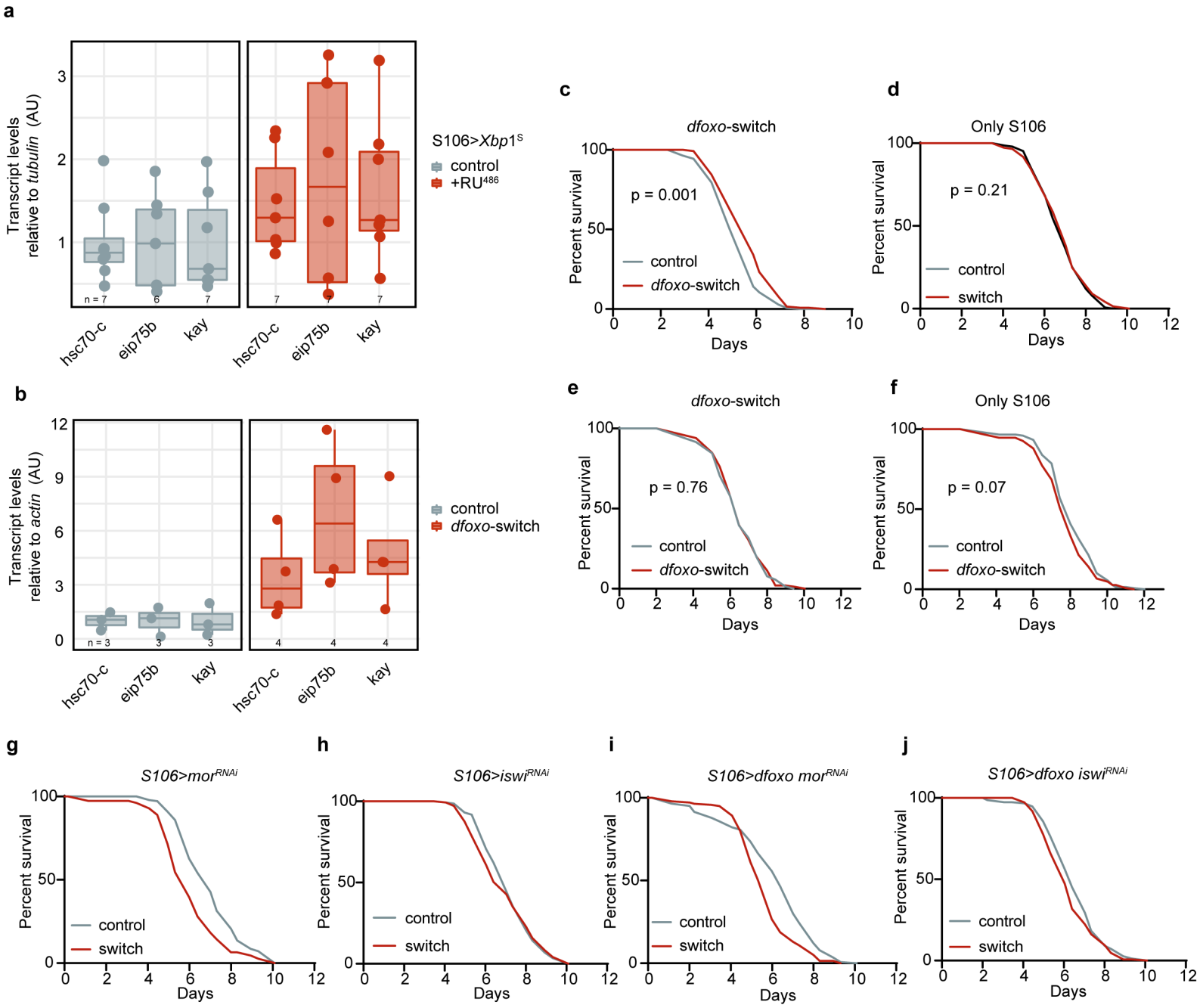
a
Transcript levels relative to tubulin (AU)
S106>Xbp1S
control
+RU486
n = 7
6
7
7
7
7
hsc70-c
eip75b
kay
b
Transcript levels relative to actin (AU)
control
dfoxo-switch
n = 3
3
3
4
4
4
c
dfoxo-switch
p = 0.001
Percent survival
Days
d
Only S106
p = 0.21
control
switch
e
p = 0.76
f
p = 0.07
g
S106>morRNAi
h
S106>iswiRNAi
i
S106>dfoxo morRNAi
j
S106>dfoxo iswiRNAi

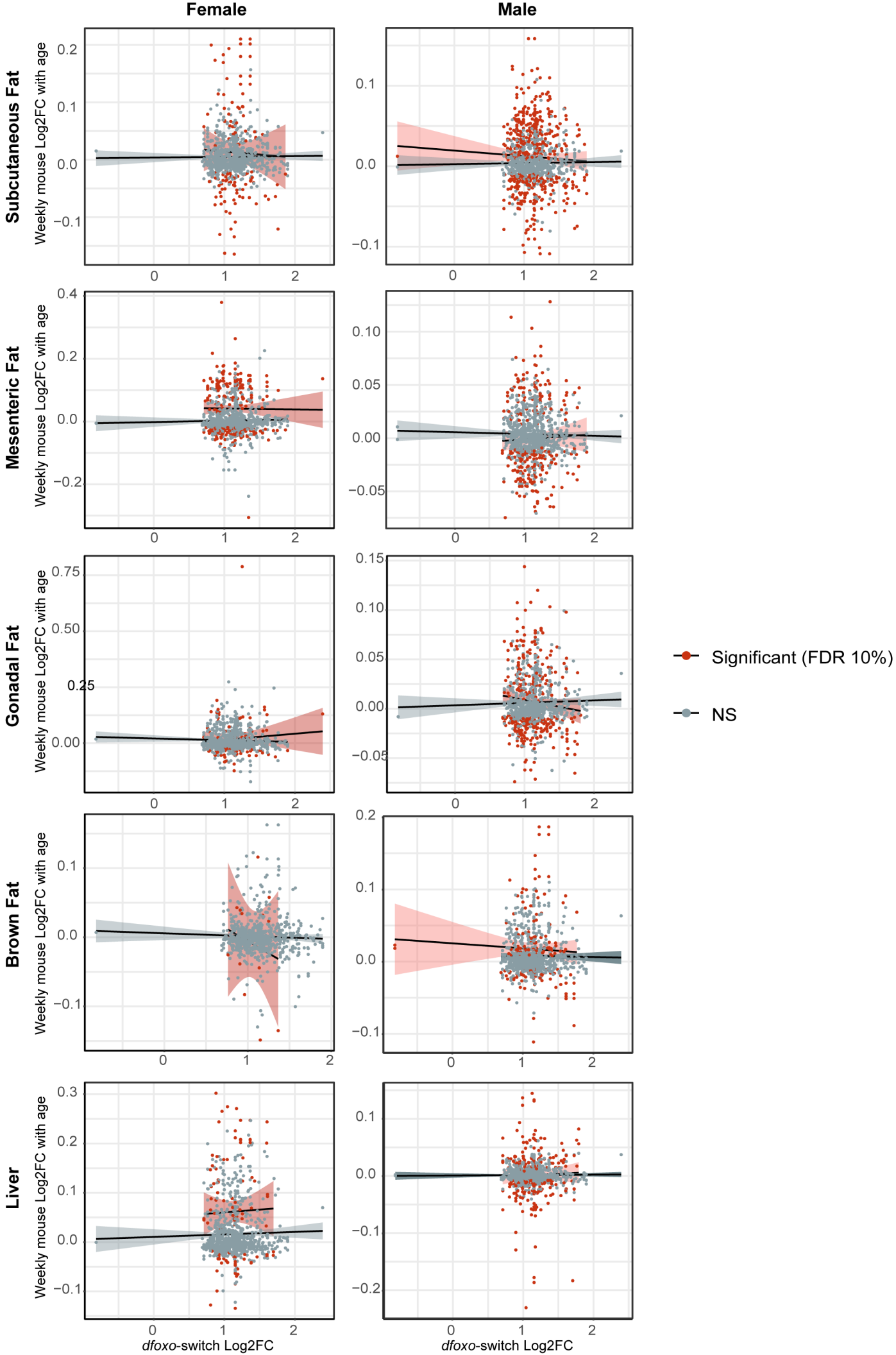
Female
Male
Subcutaneous Fat
Mesenteric Fat
Gonadal Fat
Brown Fat
Liver
Weekly mouse Log2FC with age
dfoxo-switch Log2FC
Significant (FDR 10%)
NS